VASOACTIVE MEDIATORS UNDERLYING CORONARY TONE REGULATION AND DYSREGULATION

By
Maggie Meei-Fann Kuo

A dissertation submitted to Johns Hopkins University in conformity with the requirements for the degree of Doctor of Philosophy

ABSTRACT

This dissertation illustrates the role of nitric oxide (NO) in regulating coronary tone and how impairment of NO bioavailability not only influences coronary vasoregulation but also the roles of other vasoactive mediators, namely the endothelial-derived hyperpolarizing factor (EDHF), hydrogen sulfide (H_2S).

To investigate coronary function in a physiological setting, a novel technique using high-resolution ultrasound was developed to measure coronary vasodilatory response *in vivo*. With this method, coronary vasodilatory function was evaluated in terms of increase in coronary blood flow velocity. Vasorelaxation was induced by intravenous infusion of adenosine triphosphate and by increasing myocardial demand with β-adrenergic receptor agonist dobutamine. This approach was further adapted to measure ascending aortic stiffness *in vivo*, a systemic parameter that influences coronary function. Aortic diameter was measured by ultrasound while aortic pressure was measured invasively by pressure catheter. Vasoactive drugs were infused to modulate aortic pressure to obtain a pressure-diameter relationship of the ascending aorta.

These ultrasound-based techniques were then applied to investigating the effects of ionizing radiation exposure on coronary artery function. Rats exposed to ionizing radiation exhibited reduced coronary flow *in vivo*. Decreased coronary flow was associated with both decreased aortic diastolic pressure and elevated superoxide content in the coronary artery. Reduced diastolic pressure was attributed to decreased heart rate. Reduction of superoxide production by xanthine oxidase inhibition partially restored basal coronary flow and coronary superoxide content. However, *in vivo* vasodilatory response was not improved. Moreover, endothelial function was preserved in irradiated rats. These findings support that radiation-associated coronary artery disease is initiated by an increase in superoxide level, which leads to

reduced NO bioavailability and diminished coronary vasodilatory response *in vivo*. The data further suggest that excess superoxide production precedes coronary endothelial dysfunction characteristic of coronary artery disease.

Next, the role of endogenously produced H_2S in coronary tone vasoregulation and the interaction between NO and H_2S were examined. Both cystathionine gamma lyase (CSE) and 3-mercaptopyruvate sulfurtransferase (MPST), the enzymatic producers of H_2S in the vasculature, were detected in human coronary endothelial cells and rat coronary arteries. *In vitro* measurement of H_2S production showed that the rat coronary artery can produce H_2S through the MPST pathway but not through the CSE pathway. Both pharmacologic inhibition and genetic deletion of CSE did not alter coronary vasodilatory function *in vivo,* supporting that CSE-produced H_2S does not have a significant role in coronary vasoregulation. *Ex vivo* coronary vasoreactivity response to MPST substrate 3-mercaptopyruvate (3-MP) was similar to the vasoreactivity response to H_2S donor sodium hydrosulfide (NaHS), supporting that vasoactive effects of 3-MP were through MPST-mediated production of H_2S. The data demonstrate that H_2S production in the coronary artery is mediated by MPST and not CSE, contrary to other vascular beds where CSE has a significant role. The data further show that the vasoactive effect of H_2S is NO dependent: H_2S induces coronary vasoconstriction in the presence of NO and vasorelaxation in the absence of NO. Vasoconstrictive effects of H_2S appear to be due to its scavenging of NO and the resulting decrease in NO bioavailability.

This dissertation illustrates how altering the bioavailability of NO not only influences coronary vasodilatory function but also the roles of other vasoactive mediators in coronary vasoregulation. This dissertation further demonstrates the significance of *in vivo* influences on vascular function and the power of implementing a multi-level approach in studying vascular

function. Changes in cellular signaling can be correlated to changes in physiological function, providing a more complete representation of vascular function after the introduction of a pathogenic stimulus.

ACKNOWLEDGEMENTS

This dissertation reflects not only my efforts, but the efforts of my colleagues who had supported me over the past six years. Without their mentoring and guidance, I would not have been able to accomplish what I did. I would like to specifically acknowledge Dr. Caitlin Torgerson for teaching me the ways of vascular physiology; Dr. Gautam Sikka for his technical guidance; Drs. Jae Hyung Kim and Judy Delp for teaching me microvessel work; Drs. Lars Sorensen, Iraklis Pozios, Hong Chang Luo, and Julia Gronros for helping me get the ultrasound up and running; and Dr. Deepesh Pandey for introducing me to cells and biochemistry. I also am incredibly grateful for my colleagues who ran experiments for my projects, particularly the ones with data that will never see the light of day: Dr. Dinani Armstrong, Dr. Jong Taek Park, Dr. Sung Yong Park, Ms. Alina Park, and Ms. Simran Jandu. Finally, I want to thank my committee members: Dr. Artin Shoukas for his academic guidance; Dr. Lakshmi Santhanam for her moral support; and my thesis advisor, Dr. Dan Berkowitz, for providing this environment that allowed me to come across so many wonderful people during my time here.

TABLE OF CONTENTS

LIST OF FIGURES

LIST OF ABBREVIATIONS

Ach	Acetylcholine
ATP	Adenosine triphosphate
CSE	Cystathionine gamma lyase
Dob	Dobutamine
EDHFs	Endothelium-derived hyperpolarizing factors
eNOS	Endothelial nitric oxide synthase
Gy	Gray
H_2S	Hydrogen sulfide
L-NAME	L-NG-nitroarginine methyl ester
MPST	Mercaptopyruvate sulfertransferase
NaHS	Sodium hydrosulfide
NO	Nitric oxide
OBAA	4-4(-octadecylphenyl)-4-oxobutenoic acid
ROS	Reactive oxygen species
SNP	Sodium nitroprusside

PREFACE

Because oxygen extraction in the myocardium is maximal, increased metabolic demand of the myocardium can only be matched by increasing coronary blood flow. Blood flow can only be increased by vasodilation of the coronary artery. Impaired vasodilatory response of the coronary vasculature therefore results in insufficient supply of blood and oxygen, leading to myocardial ischemia, as documented in patients with coronary artery disease. Identifying and characterizing mechanisms underlying coronary tone regulation is therefore of clinical relevance.

A sequence of events occurs to result in vasorelaxation of the coronary artery (Fig. P.1). The cascade is initiated by an external stimulus, such as neurohumoral release of acetylcholine, myocardial release of adenosine, and red blood cell release of adenosine triphosphate (ATP). These factors bind to their corresponding receptors on the endothelium and stimulate the endothelium to produce vasodilators. The three vasodilating mediators produced are nitric oxide (NO), prostanoids, and endothelium-derived hyperpolarizing factors (EDHFs). NO is produced predominantly by endothelial nitric oxide synthase (eNOS) from L-arginine. Prostanoids are produced from arachidonic acid mainly by cyclooxygenase. Prostanoids can be dilating or constricting: the overall vasoactive effect depends on which influence is more dominant. EDHFs are produced from a variety of sources, including cystathionine gamma lyase (CSE) and 3-mercaptopyruvate sulfurtransferase (MPST). Each type of vasoactive mediator has been demonstrated to be involved in coronary vasorelaxation, including maintaining baseline tone and mediating metabolic demand-induced or flow-induced vasodilation. Coronary vasorelaxation is therefore a concerted effect. The vasoactive mediators then stimulate pathways in the vascular smooth muscle cell that ultimately result in the opening of potassium (K^+) channels, causing hyperpolarization and vasorelaxation of the smooth muscle cells. NO acts through guanylyl

cyclase and cyclic guanosine monophosphate (cGMP) while the vasodilating prostanoids act through adenylyl cyclase and cyclic adenosine monophosphate (cAMP). EDHFs act directly on the K^+ channels.

Impaired vasodilatory response theoretically can arise at each stage: decreased external stimuli release, impaired endothelial production or decreased bioavailability of vasodilating mediators, or dysregulated downstream signaling in the vascular smooth muscle cells. Cardiovascular disease has been established to result from impaired endothelial function, leading to diminished production and bioavailability of vasodilators, notably NO, in the vasculature. This dissertation focuses on the role of NO in coronary tone regulation and examines how impairment of NO influences coronary vasodilatory function and the roles of other vasoactive mediators, specifically a novel EDHF hydrogen sulfide (H_2S). Chapter 1 describes two novel approaches for measuring vascular function *in vivo* in mouse and rat models using ultrasound imaging. Section 1.1 describes a technique for measuring coronary vasodilatory function and Section 1.2 describes a technique for measuring ascending aortic stiffness, a systemic parameter that influences coronary function. Chapter 2 investigates the effects of ionizing radiation exposure on coronary artery function and NO bioavailability. Chapter 3 examines the role of endogenously produced H_2S in coronary tone vasoregulation and the interaction between H_2S and NO.

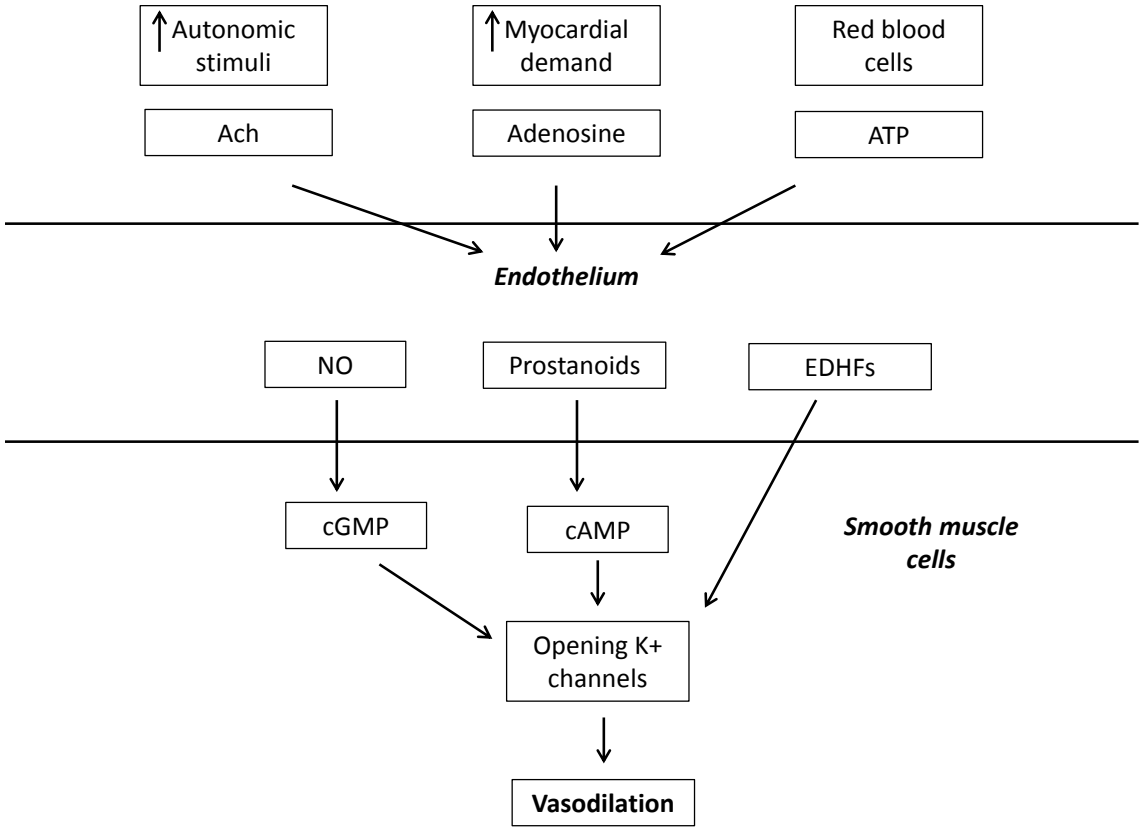

Figure P.1. Schematic of signaling cascade that leads to vasodilation of the coronary artery.

CHAPTER 1: MEASURING VASCULAR FUNCTION *IN VIVO* USING ULTRASOUND IN MOUSE AND RAT MODELS

1.1 MEASURING CORONARY VASODILATORY FUNCTION *IN VIVO*

1.1.1. INTRODUCTION

Vascular function is generally evaluated by the vessel's relaxation response to vasodilating drugs. The standard approach to characterizing vasorelaxation behavior experimentally is by myography in which the vessel is excised from the animal and experiments are performed directly on the vessel. Two types of myography set-ups exist: wire myography that records the tension produced by vessel when it constricts using a force transducer, and pressure myography that tracks the diameter of the vessel optically with a video camera. The experimental procedure is the same for either set-up. The vessel is first pre-constricted with a vasoconstricting agent, for instance phenylephrine or prostaglandin F2α. Increasing doses of a vasodilator are then added to relax the vessel to obtain a dose-dependent vasorelaxation response. On the wire myograph, vessel constriction produces an increase in measured tension and as the vessel relaxes, tension decreases. On the pressure myograph, vasoconstriction results in a decrease in vessel diameter and diameter increases as the vessel relaxes. Cellular function can be evaluated by using drugs that induce vasodilation through specific pathways. Acetylcholine (Ach) is commonly used to stimulate the endothelium to induce vasorelaxation. Sodium nitroprusside (SNP), a donor of NO, is used to stimulate the smooth muscle cells.

Endothelial function can be assessed by comparing the endothelial-mediated vasorelaxation response with the endothelial-independent response. Impaired endothelial-dependent relaxation, either in terms of decreased sensitivity to Ach or diminished maximal Ach-

induced vasodilation or both, in the presence of intact endothelial-independent relaxation support altered endothelial function. Impaired endothelial-dependent relaxation combined with impaired endothelial-independent relaxation, however, would be inconclusive as it would not be clear if endothelial function was impaired or if smooth muscle function was impaired.

Clinically, coronary artery health is measured in patients by administering a coronary vasodilator, such as adenosine or adenosine triphosphate (ATP) *[1]*, to induce maximal coronary vasodilation. Vasodilation is measured as the increase in coronary flow velocity. Coronary flow velocity during maximal vasodilation, hyperemia, is normalized to coronary flow at baseline. This ratio is called coronary flow velocity reserve (CFVR). Coronary vasodilation also is induced by increasing myocardial oxygen demand through exercise or by pharmacologic intervention, such as with β-adrenergic agonist dobutamine. Patients with coronary artery disease display decreased maximal vasodilation, which manifests as decreased hyperemic flow velocity, resulting in a lower CFVR value.

Although measuring coronary vasorelaxation *ex vivo* allows for more precise mechanistic investigations, evaluating vasorelaxation response *in vivo* provides a physiologically representative indication of coronary function. This section describes a novel technique for measuring coronary vasodilatory function in mouse and rat models by combining the *ex vivo* approach for measuring vasorelaxation response with the technique used clinically to assess coronary function in patients. Coronary vasorelaxation is measured through increase in flow velocity using ultrasound. Vasorelaxation is induced by intravenous infusion of ATP and by increasing myocardial demand with dobutamine. Because vasodilatory function can be altered in terms of both sensitivity to the vasodilator and the degree of maximal vasodilation, obtaining a

vasorelaxation response offers more conclusive data compared to measuring only maximal vasorelaxation.

1.1.2. METHODS

1.1.2.1. Transthoracic echocardiography

Coronary flow velocity is measured *in vivo* using transthoracic echocardiography as previously described *[2]*. The animal is anesthetized with 1.5% isoflurane. Chest hair is removed by depilatory cream. The animal is secured onto a heated platform to monitor ECG, heart rate, and body temperature. Coronary flow velocity is measured using the Vevo 2100 (Visual Sonics) and a 40 MHz transducer (Visual Sonics). The ultrasound station set-up is shown in Fig. 1.1.1.

The transducer is positioned laterally on the left side of the animal to obtain an image of the left ventricle, left atrium, and aorta. From this view, the left coronary artery is visualized by color flow Doppler (Fig. 1.1.2). Flow velocity profile of the blood flow through the coronary artery is captured by pulse wave velocity. The transducer is mounted on a stand (Visual Sonics) to measure flow velocity from the same location for the entire experiment. The difference in angle between blood flow and ultrasound beam is accounted for with angle correction done on the Vevo mainframe.

1.1.2.2. Coronary vasoreactivity

Catheters are custom-made by attaching a 30-gauge needle (BD) to size PE-10 polyethylene tubing (BD). The animal is warmed for ~5 minutes to dilate the peripheral veins. A tourniquet is tied at the base of the tail to visualize the lateral tail vein. The needle is inserted into the tail vein and the catheter is connected to a syringe placed in a syringe pump (Harvard

Apparatus). Vasodilating drugs are administered intravenously through the catheter. Increase in coronary artery diameter corresponds with an increase in flow velocity. Dose of drug administered is controlled with a syringe pump by adjusting infusion rate (Harvard Apparatus).

Coronary vasorelaxation is induced by intravenous infusion of adenosine triphosphate (ATP, Sigma) or β-adrenergic agonist dobutamine (Dob, Hospira). ATP is administered to evaluate agonist-induced coronary vasorelaxation and dobutamine to evaluate metabolic demand-mediated vasorelaxation. Working concentration of ATP is 0.5 mg/mL. ATP is infused at 20, 40, 80, and 160 μg/kg/min for 1 minute per dose. Coronary flow velocity is allowed to return to baseline between each dose. The working concentration of dobutamine is 0.2 mg/mL. Dobutamine is infused at 5, 10, 20, and 30 μg/kg/min at 2 minutes per dose. All drugs are prepared in a heparinized 0.9% saline solution. Peak diastolic flow velocities of three cardiac cycles are measured for data analysis.

1.1.3. RESULTS

Modified long axis view obtained to visualize the left main coronary artery is shown in Figure 1.1.2. Increasing dose of ATP causes a dose-dependent increase in coronary flow velocity, as shown in Figure 1.1.3. Flow velocity at baseline is shown in (1.1.3A), at 40 μg/kg/min is shown in (1.1.3B), and at 160 μg/kg/min is shown in (1.1.3C). Peak flow velocity can be plotted against dose of ATP, as shown in Figure 1.1.4A, and dose of dobutamine, as shown in Figure 1.1.4B, to show agonist-dependent and myocardial demand-dependent increase in coronary flow.

1.1.4. DISCUSSION

This technique is a physiologically-relevant functional assessment of coronary health. Moreover, because drugs are infused through a catheter inserted into the tail vein, the procedure is non-invasive and allows for multiple time-point measurements in the same animal. When combined with *ex vivo* and *in vitro* assessment of coronary function, a complete evaluation of coronary health can be obtained.

One disadvantage of this method is that cellular function cannot readily be evaluated as with *ex vivo* myography techniques. ATP causes endothelial-dependent coronary vasodilation *ex vivo [3]*. *In vivo*, however, ATP is hydrolyzed by ectonucleotidases to adenosine, adenosine monophosphate (AMP), and adenosine diphosphate (ADP) *[4]*. Vasodilation that occurs *in vivo* with ATP administration results from the combined effect of adenosine, AMP, ADP, and ATP. ATP and ADP act through the P2Y purinergic receptors while adenosine and AMP act through the P1 purinergic receptors *[5]*. These receptors are expressed in both endothelial and vascular smooth muscle cells, so vasodilation occurs through both endothelial-dependent and – independent pathways *[6]*.

Ach could be administered to examine endothelial function. However, during our studies, we observed that systemic administration of Ach resulted in decreased flow velocity, indicating coronary vasoconstriction. Moreover, flow velocity changes are in the range of 100 mm/s, which is within the margin of uncertainty of the ultrasound measurements. Nevertheless, ATP and dobutamine-induced increase in myocardial demand are physiologically-relevant stimuli so coronary function measured through the administration of these drugs provides an accurate indication of *in vivo* coronary function.

1.1.5. FIGURES

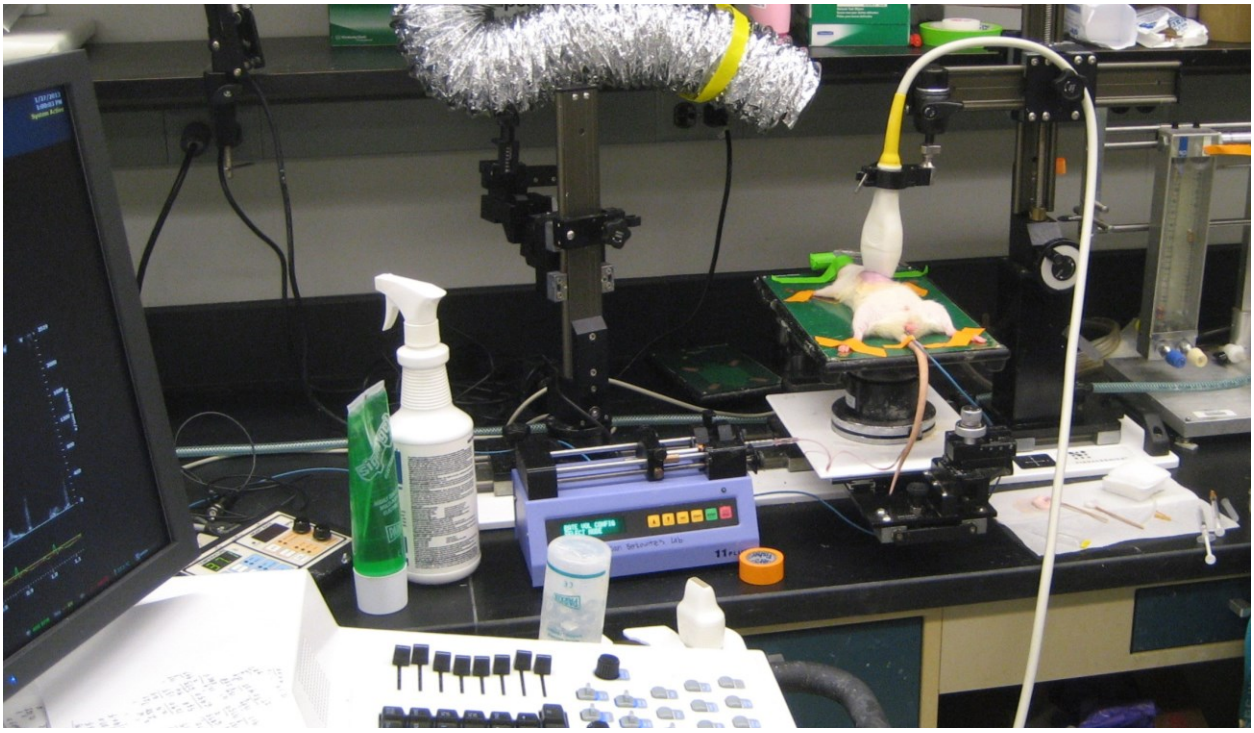

Figure 1.1.1. Ultrasound station set-up. The Vevo 2100 is used to for ultrasound experiments. The mainframe is in the foreground. The probe is mounted on the rail system so that measurements can be made from the same location for the duration of the experiment. A catheter is inserted into the tail vein for intravenous administration of vasodilating drugs. Dose of drug is controlled by changing infusion rate using a syringe pump (in purple).

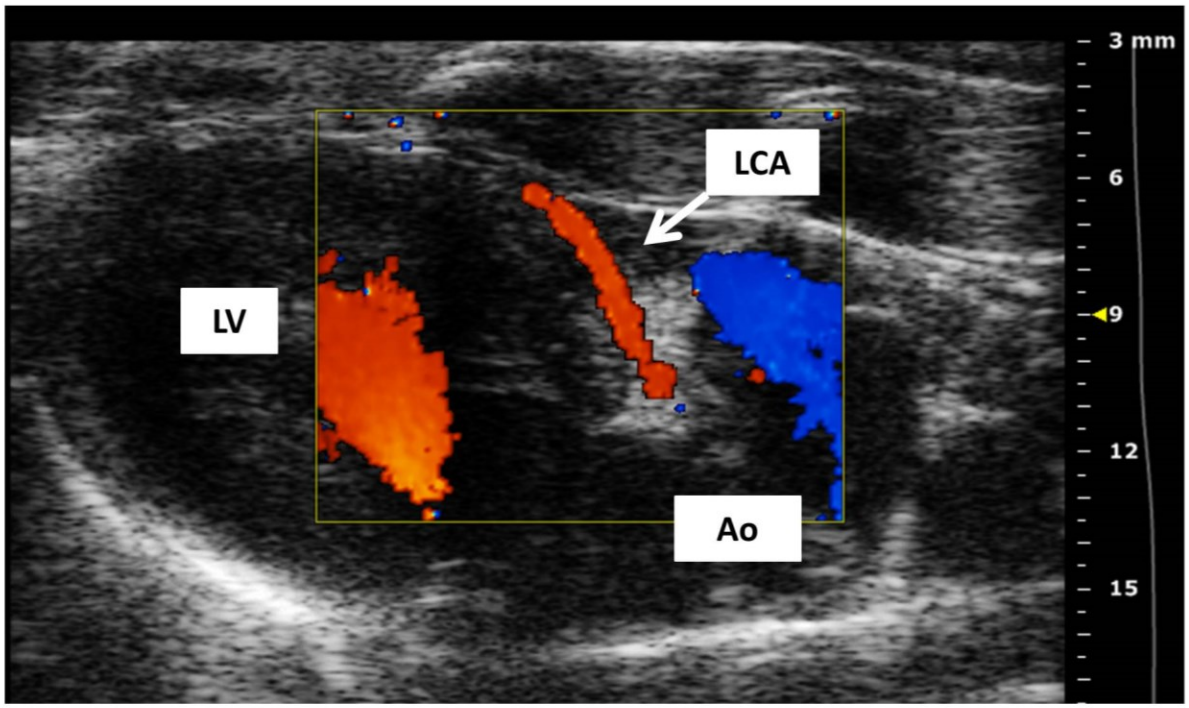

Figure 1.1.2. Locating the left descending coronary artery. Ultrasound probe is placed on the left side of the animal to obtain a long axis view of the aorta (Ao) and left ventricle (LV). The left coronary artery (LCA) is visualized by color Doppler and can be identified as coming off of the aorta, crossing the pulmonary artery. Flow velocity is measured from the left main section.

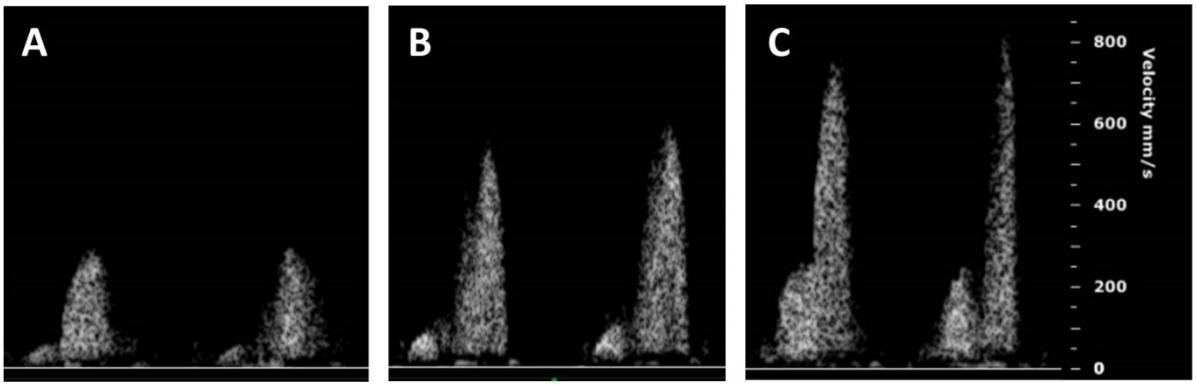

Figure 1.1.3. Coronary blood flow velocity profile. Blood flow velocity profile is captured by pulse wave velocity. Both systolic and diastolic portions are visible. (A) shows a representative flow velocity profile at baseline. Increasing dose of vasodilator increases both systolic and diastolic flow velocities, although the increase in diastolic flow velocity is more dramatic. (B) shows the flow velocity profile at 40 μg/kg/min ATP and (C) shows the flow velocity profile at 160 μg/kg/min ATP.

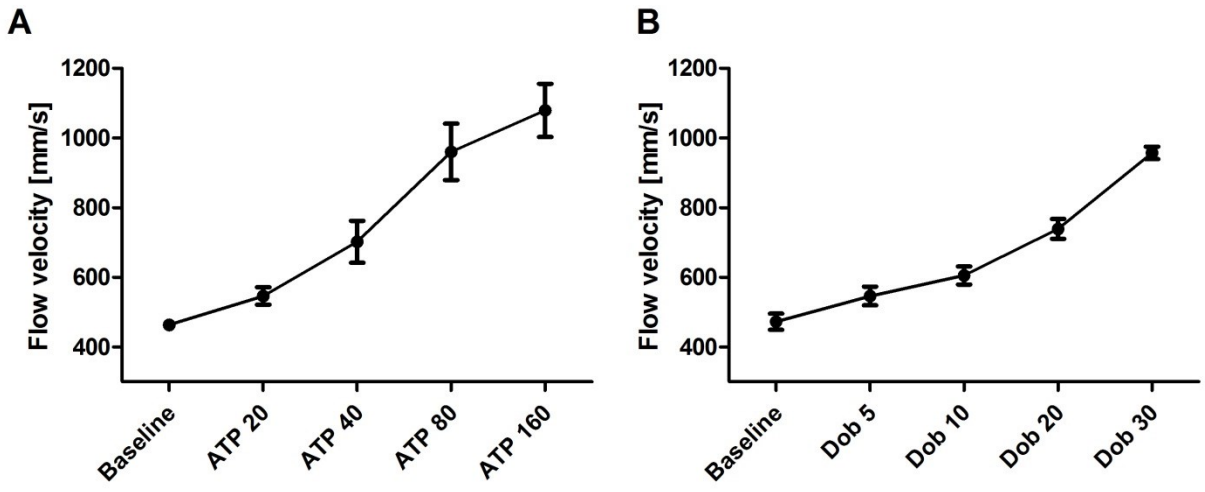

Figure 1.1.4. Dose-dependent increase in peak diastolic flow velocity. Peak diastolic flow velocity is measured for data analysis. Increasing ATP dose causes a dose-dependent increase in flow velocity (A). Increasing dobutamine (Dob) dose similarly causes a dose-dependent increase in flow velocity (B).

1.2 DETERMINING *IN VIVO* ASCENDING AORTIC STIFFNESS FROM ITS PRESSURE-DIAMETER RELATIONSHIP

1.2.1. INTRODUCTION

Increased aortic stiffness is a hallmark of cardiovascular disease. Aging *[7]*, smoking *[8]*, diabetes *[9]*, hyperlipidemia *[10]*, and other risk factors of cardiovascular disease have been shown to increase aortic stiffness. Epidemiological studies have further demonstrated aortic stiffness as a powerful independent predictor of the onset of coronary heart disease and stroke, as well as the occurrence of cardiovascular events and mortality *[11-14]*. Because of the clinical and public health significance of increased aortic stiffness, current research is focused on understanding the mechanisms underlying the development and progression of vascular stiffness. Great interest therefore exists in developing accurate measures of vascular stiffness in experimental models of cardiovascular disease.

A material's stiffness can be characterized by its stress-strain relationship and quantified as elastic modulus. A linear elastic material deforms reversibly and its stress increases proportionally to strain. The aorta and the large arteries are nonlinear elastic bodies: when stretched, the stiffness of the artery does not remain constant but increases with the degree of distension. This nonlinearity in the mechanical properties of large arteries is due to the different stiffness properties of the load-bearing elements, namely elastin and collagen, that constitute the vessel wall. Elastin is highly extensible with an elastic modulus of 0.6 MPa. In comparison, collagen is very stiff with an elastic modulus of 1 GPa *[15]*. The initial stiffness exhibited by the aorta at lower strain values is attributed to elastin while the high stiffness exhibited at high strain values is due to collagen. Load is transferred from elastin to collagen as the vessel distends and

this region of load transferring is where the vascular system operates. Therefore, at physiologic pressures, arterial stiffness depends on the contribution of both elastin and collagen *[16]*.

The distribution and orientation of elastin and collagen vary by layer within the arterial wall. In the media, the elastin, collagen, and smooth muscle cells are bundled into tight helices that are layered concentrically. This arrangement allows the artery to resist high loads in the circumferential direction. The adventitia is predominantly collagen with little elastin and the collagen fibers are organized in a net-like fashion. These collagen fibers are wavy in an unstressed state and straighten out as load increases. Stiffness increases as the collagen fibers straighten out, thereby preventing the artery from overstretching and rupturing. Because of the structural organization and varying orientation of the collagen fibers, arteries are anisotropic: the stiffness exhibited depends on if the vessel is stretched longitudinally or circumferentially *[17]*. In vivo stiffness is therefore a composite of the aorta's longitudinal and circumferential stiffness.

Arterial stiffness is generally quantified in vivo as compliance or pulse wave velocity (PWV). Arterial compliance is defined as $C = \Delta D / \Delta P$ where ΔD is change in diameter and ΔP is the corresponding change in pressure. Lower values of compliance indicate stiffer vessels. Compliance is calculated from the pressure-dimension relationship of the artery and is therefore a direct measure of stiffness. As stiffness is disseminated non-uniformly in the vasculature *[18]*, compliance should be measured at the same/similar location in each subject to make meaningful comparisons between experimental groups.

The difference between compliance and elastic modulus is that elastic modulus is normalized to the material's dimensions. Compliance therefore reflects structural stiffness whereas elastic modulus reflects material stiffness. With aging, arterial wall thickness increases and elastin/collagen ratio decreases, so both structural stiffness and material stiffness are greater.

Compared to compliance, PWV is an indirect measure of arterial stiffness. PWV is the speed at which a pressure pulse travels along a length of artery and is influenced by the properties of the vessel wall. The Moens-Korteweg equation is used to model the relationship between PWV and elastic modulus: $PWV^2 = E\ h / (2\ \rho\ r)$ where E is incremental elastic modulus, h is wall thickness, ρ is blood viscosity, and r is vessel radius. A higher PWV value therefore suggests a stiffer vessel.

Compliance and elastic modulus can be measured experimentally ex vivo on an excised segment of vessel. To determine compliance, the vessel segment is mounted on a pressure myograph *[19,20]*. Pressure within the vessel is increased step-wise and the resulting change in diameter is tracked using video microscopy. Compliance is determined from the pressure-diameter data. Incremental elastic modulus can be measured by tensile testing. In these experiments, the vessel is pulled apart step-wise and force-displacement data is collected until the vessel ring breaks. Stress and strain values can be calculated and plotted to determine incremental elastic modulus. These *ex vivo* approaches can be used to evaluate changes in the passive properties that influence stiffness.

In vivo, in addition to wall content, vascular stiffness is influenced dynamically by smooth muscle tone and blood pressure *[19,21,22]*. PWV is the most widely used method for measuring in vivo aortic stiffness in experimental models. PWV can be determined non-invasively using Doppler ultrasound or applanation tonometry *[23]*. Pressure pulse is measured at two separate locations and the time required for the pulse to traverse the distance is the pulse wave velocity. Because PWV is measured over a length of aorta, it is an averaged value of stiffness. Large arteries are nonlinear elastic, so stiffness and therefore PWV will vary with arterial pressure. A higher PWV value could therefore arise from increased stiffness or elevated

pressure. PWV values therefore must be normalized to blood pressure to derive conclusions about the vessel's stiffness. Measurement methods that incorporate the influence of blood pressure with the passive properties of the vascular wall and the effects of vasoactive mediators that alter tone would yield a physiologically relevant index of arterial stiffness. This approach is implemented by measuring PWV invasively using a catheter with two pressure sensors separated at a fixed distance *[19]*. This dual-pressure catheter is inserted into the aorta and vasoactive drugs such as phenylephrine or sodium nitroprusside are infused intravenously through a venous catheter to raise and lower arterial pressure.

This protocol describes a method to determine aortic stiffness in vivo from its pressure-dimension relationship in a mouse model. This approach offers several advantages over the invasive PWV measurement. Stiffness indices, such as compliance, can be calculated from the pressure-dimension data collected by this procedure. Moreover, this technique allows for measurement of local aortic stiffness because stiffness is measured from a single location. This approach is particularly useful in measuring ascending aortic stiffness as the short length of this region makes a PWV measurement difficult to obtain. Research interest exists specifically in the ascending aorta because its mechanical properties influence the perfusion of the coronary circulation and the cardiac response to vascular dysfunction.

To measure the pressure-diameter relationship of the aorta in vivo, the ascending aorta is visualized and its diameter is measured by ultrasound imaging. Aortic blood pressure is measured invasively with a pressure catheter. Blood pressure is changed incrementally by intravenous infusion of vasoactive drugs. Phenylephrine constricts blood vessels and is used to raise aortic pressure. Sodium nitroprusside dilates blood vessels and is used to lower aortic pressure. Systolic and diastolic aortic diameters and corresponding aortic pressures are measured

for each pressure increment. Compliance can be calculated from the pressure-diameter data collected.

1.2.2. METHOD

This protocol has been approved by the Institutional Animal Care and Use Committee at Johns Hopkins University.

1. Preparation of solutions, materials, and animal

1.1) Prepare a 300 μg/ml solution of phenylephrine (PE) and 300 μg/ml solution of sodium nitroprusside (SNP) in 0.9% saline. Prepare a separate heparin-saline solution by mixing 1 mL of 1000 U/mL heparin into 10 mL 0.9% saline. Note: Drugs should be at room temperature before use.

1.2) Make the catheter for intravenous drug infusion from two 30G x ½" hypodermic needles and PE 10 polyethylene tubing. To make the catheter, insert one needle into one end of the tubing. Remove the needle portion of the other hypodermic needle and insert the blunt end into the other end of the tubing. Attach the catheter to a 1 ml syringe and fill the catheter with the heparin-saline solution.

1.3) Place mouse in the anesthesia induction chamber containing 2-2.5% isoflurane in 100% oxygen. Leave the mouse in the induction chamber until it is unresponsive to external stimuli. Remove the mouse from the induction chamber and place it on the heated electrocardiogram (ECG) pad. Maintain the animal at 2% isoflurane.

1.4) If necessary, apply vet ointment or saline solution to the animal's eyes to prevent dryness during the procedure.

2. Insertion of catheter into tail vein

2.1) Since the tail veins are located laterally on both sides of the tail, place the animal on its side for better access. Secure the mouse onto the ECG pad with tape. Make sure the animal is kept warm to promote vasodilation of the tail veins.

2.2) Using a piece of silastic tubing as a tourniquet, tie the tourniquet around the base of the tail. Tie the tourniquet tight enough to collapse the veins but not enough to cut off the arterial circulation. After 2-3 minutes, the vein should bulge out and become more visible.

2.3) Gently pull the tail taut. Bend the tail at an angle with one hand and hold the needle parallel to the tail with the other. Pierce the needle where the tail is bent through the skin into the vein. Blood will push back into the catheter if the needle is inserted into the vein.

2.4) Place one drop of tissue glue where the needle is inserted to secure the catheter. Remove the tourniquet and confirm patency by injecting saline with little resistance.

3. Insertion of blood pressure catheter through femoral artery

3.1) Place the pressure catheter into a 30 ml syringe filled with distilled water and connect the catheter to the pressure control unit. The catheter should soak in water, plugged in, for 30-45 minutes during the set-up and surgery procedures.

3.2) Place the animal supine and tape its paws onto the ECG pad. Apply depilatory cream on the chest and area over the femoral artery.

3.2.1) Wait 3-5 minutes and remove cream and hair. Hair must be thoroughly removed from the chest to prevent artifacts during the ultrasound. Wipe both the chest and hind limb regions with a moistened pad to remove excess depilatory cream.

3.3) Using fine scissors, make an incision in the skin above the location of the femoral artery. Dissect through the subcutaneous fat tissue to reveal the femoral artery. The femoral artery is partially covered by the abdomen. Use hemostats to move the abdomen away.

3.4) Using fine forceps, separate the nerve away from the artery-vein bundle. Gently pierce through the sheath around the artery-vein bundle to separate the artery from the vein. Pass one suture around the artery at the proximal end and place two sutures at the distal end.

3.5) Securely knot the most distal suture to stop distal blood flow. Use hemostats to pull the proximal suture to temporarily stop blood flow into the femoral artery. Use microscissors to make a small incision into the femoral artery. Make the incision near the distal knot.

3.6) Calibrate the data acquisition software to the catheter using the calibration settings on the pressure control unit. Switch the pressure control unit back to reading the transducer and balance the pressure catheter so that the catheter outputs 0 mmHg in the water-filled syringe.

3.7) Insert the catheter into the femoral artery. Open the incision with fine forceps with one hand and insert the catheter head into the artery with the other hand. Knot the middle suture around the catheter wire to secure the catheter into the artery. Relax the proximal suture and advance the catheter forward into the abdominal aorta. Knot the proximal suture to further secure the catheter and to prevent bleeding.

3.8) Carefully move the ECG pad with mouse, pressure catheter and saline syringe to the ultrasound imaging stage. Connect the blood pressure catheter to the pressure control unit. Place the saline syringe in the syringe pump. Allow the animal to equilibrate for 20 minutes. This period will also allow the catheter to equilibrate.

4. Measuring aortic diameter over a range of blood pressures

4.1) Reduce isoflurane to 1.5%. Visualize the ascending aorta longitudinally on B-mode using a long axis view. Mount the transducer onto the rail system so that the same view is maintained for the duration of the experiment.

4.2) On the ultrasound mainframe, place the M-mode cursor over the section of aorta to be tracked. Track the aortic diameter change over the cardiac cycle using M-mode.

4.3) Change the saline in the syringe to the PE solution and place the syringe into the syringe pump.

4.3.1) Record M-mode at baseline aortic pressure. Begin infusion at 360 µg/kg/min and infuse for 1 minute for aortic pressure to reach a plateau. For a 25 g mouse, this dose equates to 30 µl/min.

4.3.2) Record the M-mode, then stop the infusion, and wait 2 minutes for blood pressure to return to baseline.

4.4) Lower infusion rate to 240 µg/kg/min. For a 25 g mouse, this dose equates to 20 µl/min. Start infusion, infuse for 1 minute for blood pressure to plateau, and record M-mode. Stop the infusion, and wait 2 minutes for blood pressure to return to baseline.

4.5) Repeat step 4.4 for 120 µg/kg/min PE (10 µl/min for a 25 g mouse).

4.6) Replace PE with saline and infuse the saline at the rate used for the 360 µg/kg/min infusion (30 µl/min for a 25 g mouse). Infuse for 2-3 minutes, until further infusion does not produce an increase in aortic pressure and pressure is returning to baseline. Wait 5 minutes for the blood pressure to stabilize at baseline.

4.7) Replace saline with SNP.

4.7.1) Record M-mode at baseline aortic pressure. Begin infusion at 240 µg/kg/min (20 µl/min for 25 g mouse)and infuse for 1 minute. When aortic pressure reaches a plateau, record the M-mode. Stop the infusion and wait 2 minutes for blood pressure to return to baseline.

4.8) Lower infusion rate to 120 µg/kg/min (10 µl/min for 25 g mouse). Start infusion, infuse for 1 minute for blood pressure to plateau, and record M-mode. Stop infusion and wait 2 minutes for blood pressure to return to baseline.

4.9) Repeat step 4.8 for 60 µg/kg/min SNP (5 µl/minfor 25 g mouse).

5. Terminating the experiment

5.1) To euthanize the animal, increase isoflurane to 4%. When breathing has slowed, usually in 1-2 minutes, cut through the sternum with scissors to open the thoracic cavity and expose the heart.

5.2) Grasp the heart with medium forceps and excise it from the body by cutting at the ascending aorta with scissors.

1.2.3. RESULTS

A longitudinal image of the left ventricle and ascending aorta is captured on B-mode, as shown in Figure 1.2.1. Alternatively, a longitudinal image of only the aorta can be obtained, as in Figure 1.2.2. The movement of the aortic wall during the cardiac cycle appears as two white lines on the M-mode, as shown in Figure 1.2.3. The aortic lumen is the area in between the lines. Aortic pressure is modulated by infusion of vasoactive drugs. PE raises the aortic pressure, as shown in Figure 1.2.4A, and SNP lowers pressure, as shown in Figure 1.2.4B. M-mode is recorded when blood pressure plateaus, 1 minute after the start of infusion. Aortic pressure is

changed incrementally through changing the dose of the drug administered, as shown in Figure 1.2.5. Dose of drug is controlled through the rate of infusion. All drug doses are in μg/kg/min. Maximum and minimum diameters are measured from the M-mode, shown in Figure 1.2.3. These diameters correspond to the systolic and diastolic aortic pressures recorded by the pressure catheter.

Systolic and diastolic diameter and pressure values of three cardiac cycles are measured at baseline and for each PE and SNP dose. The standard deviation between three diameter measurements at one drug dose ranges from 0.01 mm to 0.04 mm. Aortic diameter can be plotted against its corresponding aortic pressure to illustrate the pressure-diameter relationship, as shown in Figure 1.2.6A.

These pressure-diameter values are used to calculate aortic compliance. Arterial compliance is calculated by $C = (Dsys - Ddia) / (Psys - Pdia)$ (1)
where Dsys and Ddia are systolic and diastolic diameters and Psys and Pdia are systolic and diastolic pressures. Compliance and mean aortic pressure (MAP) are calculated at baseline and for each PE and SNP dose. Compliance is plotted against MAP to demonstrate the pressure-dependency of stiffness. Because of the nonlinear elastic behavior of the aorta, compliance decreases with increasing MAP, as seen in Figure 1.2.6B.

1.2.4. DISCUSSION

Taking diameter measurements at several pressure increments over a wide range of pressure values is necessary for accurate characterization of the pressure-diameter relationship. The upper and lower pressure limits that can be pharmacologically induced may vary by the experimental group but the ideal range is around 25 mmHg to 125 mmHg diastolic and 50

mmHg to 200 mmHg systolic. Dose of 360 μg/kg/min PE and 240 μg/kg/min SNP generally elicit the limits of the pressure range. However, dose of PE can be increased to 480 μg/kg/min and SNP to 360 μg/kg/min to verify that the limits have been reached. Working concentrations of PE and SNP can be decreased to achieve finer pressure increments. As diameter will change with aortic pressure, inducing the same pressure values between animals and experimental groups is not important.

Venous and arterial cannulation can be performed at other locations with the same outcomes. Tail vein cannulation can be challenging because of the small size of the tail vein. Moreover, the tail vein is not readily visible in dark-colored mice. The femoral vein can be cannulated as an alternative. This route may be easier since the femoral vein is more accessible. For pressure catheter insertion, besides the femoral artery, the catheter can be inserted through the carotid. The femoral artery is preferable over the carotid artery, however, because the chest region remains intact for the ultrasound imaging. Femoral artery cannulation can be more difficult because the femoral artery is smaller. Using a 1.2F catheter and introducing the catheter in the proximal femoral artery beneath the abdominal cavity will facilitate the cannulation process. Placing a few drops of a vasodilating agent like lidocaine onto the femoral artery or using a catheter introducer can also help enlarge the vessel to facilitate catheter insertion. The pressure catheter should be handled and used according to the manufacturer's instructions.

Location of the catheter within the aorta does not need to be consistent between animals as the pressure drop within the aorta is insignificant. However, placing the catheter in the abdominal aorta may be better to minimize interference with the ultrasound imaging of the thoracic aorta. Some ultrasound mainframes can record pressure real-time with the M-mode trace, thereby giving a pressure measurement for every diameter measured on the M-mode.

Unfortunately, because the location where the diameter is measured is not the same location as where pressure is recorded, a lag exists between the pressure recorded at the catheter and the actual pressure in the ascending aorta. As a result, only maximum and minimum diameter measurements can be used for the data analysis.

The primary limitation of this method is the uncertainty in measurement introduced by the aorta shifting in and out of the ultrasound plane during the cardiac cycle. Motion-introduced error is common to all imaging-based studies, including MRI and CT. Compensation strategies include using anatomical features to shift the frame of reference with the movement *[24]* and are implemented during data processing. As motion compensation software is not readily available, the investigator has to be vigilant about adjusting the location of the probe to track the shift in location of the aorta as blood pressure rises and decreases. Diameter measurements should also be taken through the center of the aorta. However, determining whether the M-mode recording location is passing through the center can be difficult to judge on the ultrasound image, especially with the aorta shifting positions. The uncertainty introduced by these limitations manifest in the degree of scatter in the data, as evident in Figure 1.2.6. Obtaining an image of the cross-section instead of longitudinal axis of the ascending aorta could be a solution. However, obtaining this view can sometimes be more challenging and the resulting M-mode trace can be less clear. The cross-sectional circumference from the B-mode image could be measured instead of the diameter from the M-mode image. However, determining when maximum and minimum circumference has been achieved will be limited by the B-mode frame rate and may be more difficult to judge than on the M-mode.

Making multiple measurements of the pressure-diameter plot and increasing experimental group size can improve accuracy of the data. The pressure-diameter data can be collected from

several locations along the chest. This protocol would first be carried out with the probe placed on one location on the chest. The aorta would then be visualized with the probe placed on another location and the protocol repeated.

Vasoactive agents used to modulate blood pressure could potentially affect aortic smooth muscle tone, which in turn would affect stiffness. However, manipulation of aortic pressure by venous return has been shown to produce similar changes in invasively measured PWV as pharmacologic manipulation in rats. These findings demonstrate that infusion of vasoactive drugs act primarily on the peripheral resistance arteries and do not significantly affect aortic smooth muscle tone *[25]*.

This protocol can be performed in rats with a few minor modifications. The chest is shaved prior to applying depilatory cream. A commercially available 27G x ½" catheter is used for drug infusion. The drug doses used to modulate aortic pressure are 40, 80, and 120 µg/kg/min PE and 40, 80, and 120 µg/kg/min SNP.

Besides the ascending aorta, regional differences in aortic stiffness can be determined with this protocol. Regional stiffness measured by this approach would be more precise than by PWV as measurements are taken from one location as oppose to two locations for PWV. However, regions along the aorta that can be measured with this technique are limited to those that can be visualized by ultrasound.

Elastic modulus can also be calculated from the data collected by this method if a wall thickness measurement can be obtained. Accurate in vivo measurement of the mouse aorta is limited by the resolution limits of current ultrasound technology. Future improvement of ultrasound technology could make in vivo wall thickness measurement more feasible. As an alternative, thickness measurements can be performed ex vivo. Pressure myography would

provide the most accurate measurements because thickness can be measured at each pressure increment.

Text reprinted with permission from Kuo MM, Barodka V, Abraham TP, Steppan J, Shoukas AA, Butlin M, et al. Measuring ascending aortic stiffness *in vivo* in mice using ultrasound. J Vis Exp 2014; e52200 *[26]*.

1.2.5. FIGURES

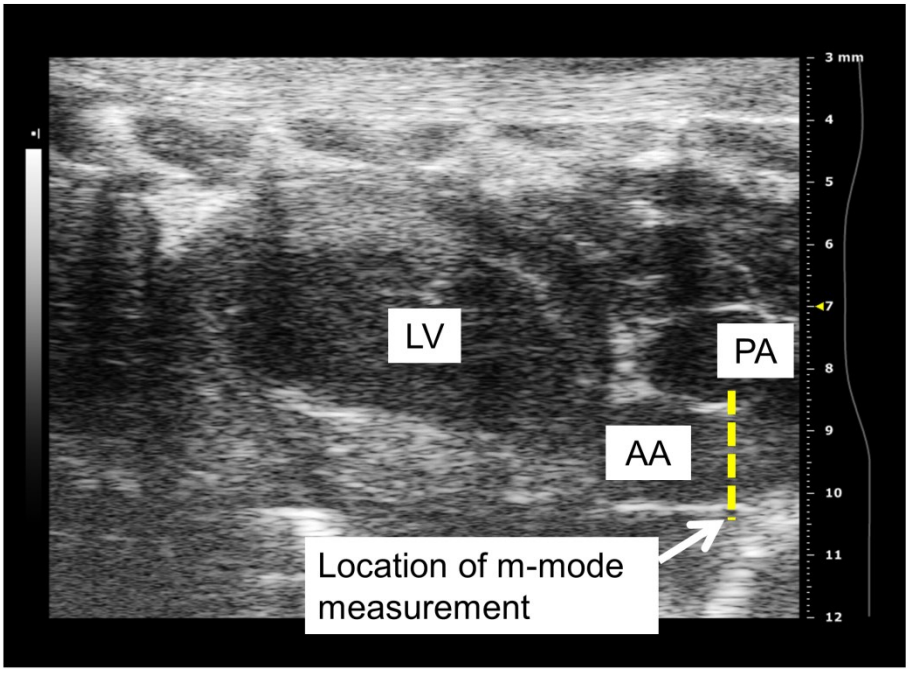

Figure 1.2.1. Longitudinal view of ascending aorta on B-mode. Diameter measurements are taken from a longitudinal image of the ascending aorta leaving the left ventricle. LV: left ventricle; PA: pulmonary artery; AA: ascending aorta. Visualization of the pulmonary artery depends on the probe placement. Aortic diameter is measured distal to the aortic valve. Frequency of the probe used to capture this image is 40 MHz.

Figure reprinted with permission from Kuo MM, Barodka V, Abraham TP, Steppan J, Shoukas AA, Butlin M, et al. Measuring ascending aortic stiffness *in vivo* in mice using ultrasound. J Vis Exp 2014; e52200.

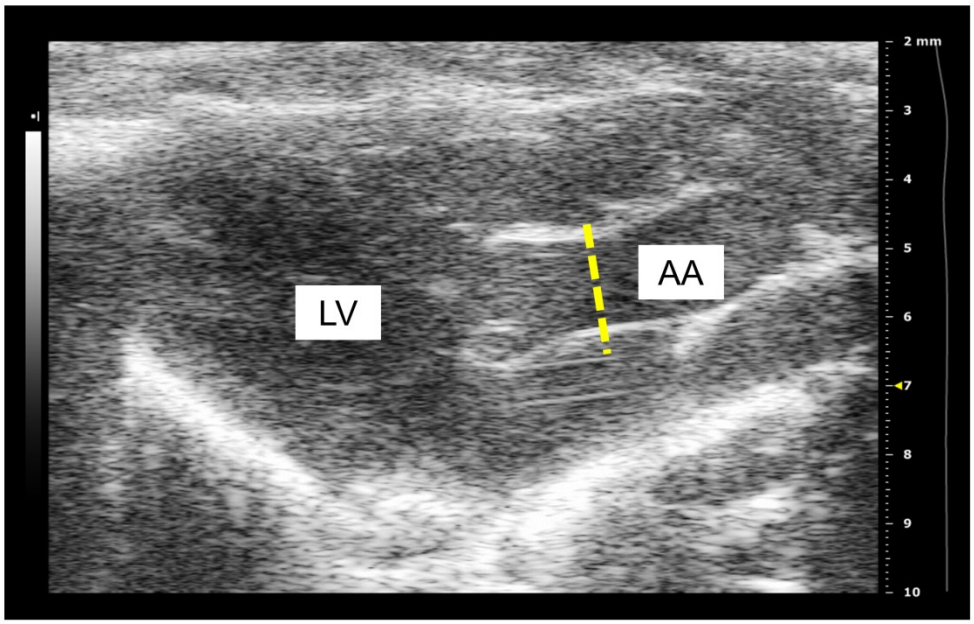

Figure 1.2.2. Alternate view of ascending aorta on B-mode. The ascending aorta is featured more prominently and the left ventricle and heart walls are less distinct. AA: ascending aorta; LV: left ventricle. Frequency of probe used to record this image is 40 MHz.

Figure reprinted with permission from Kuo MM, Barodka V, Abraham TP, Steppan J, Shoukas AA, Butlin M, et al. Measuring ascending aortic stiffness *in vivo* in mice using ultrasound. J Vis Exp 2014; e52200.

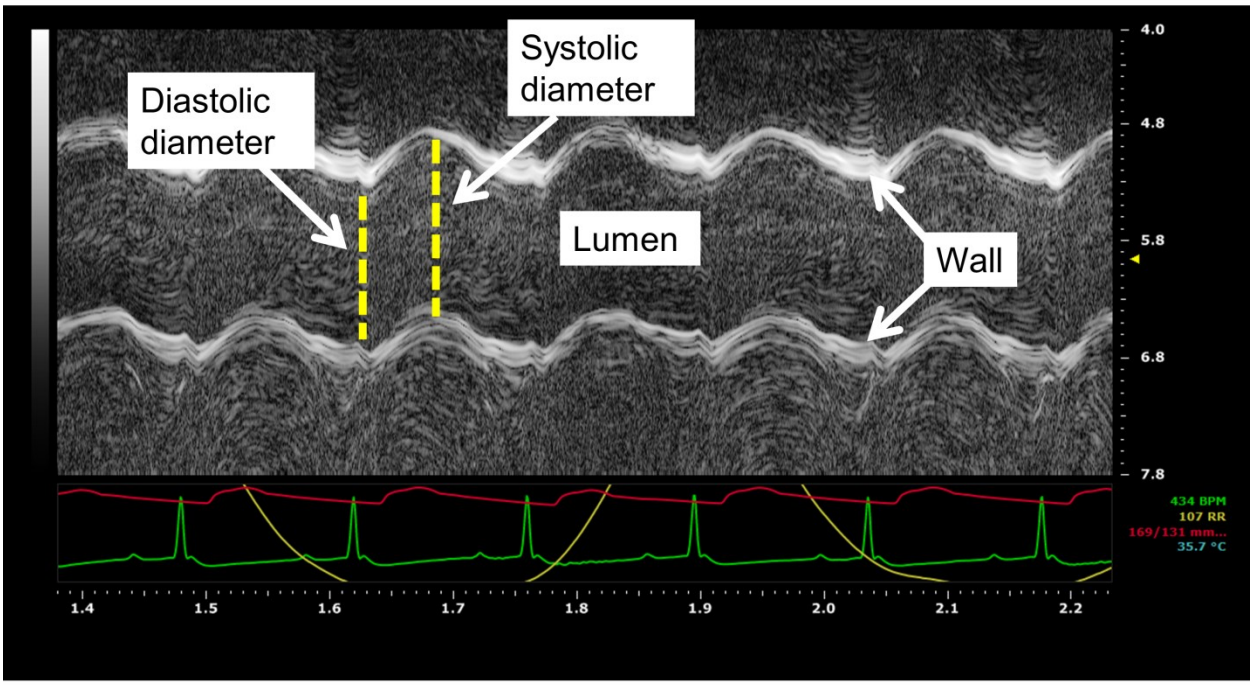

Figure 1.2.3: Aorta visualized on M-mode. Aortic diameter is measured from the M-mode image. The movement of the aortic wall appears as two wavy lines. The space in between the two lines is the aortic lumen. Systolic and diastolic aortic diameters of three cardiac cycles are measured from the M-mode. In this image, aortic pressure recorded by the pressure catheter, ECG signal, and respiratory cycle are displayed in red, green, and yellow on the M-mode. Probe frequency used to record this image is 40 MHz and the acquisition sweep speed is 1200 Hz.

Figure reprinted with permission from Kuo MM, Barodka V, Abraham TP, Steppan J, Shoukas AA, Butlin M, et al. Measuring ascending aortic stiffness *in vivo* in mice using ultrasound. J Vis Exp 2014; e52200.

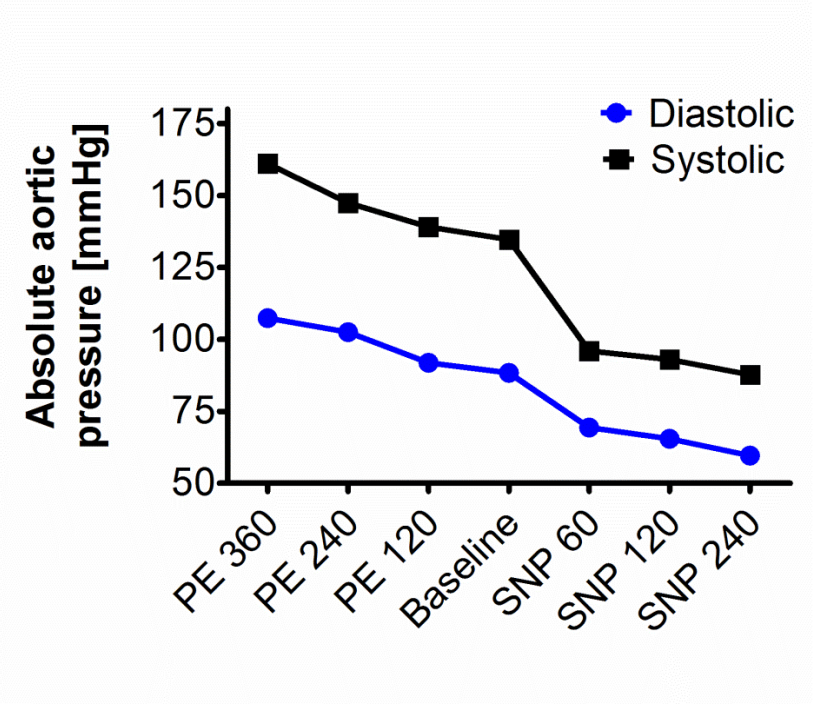

Figure 1.2.4: Modulating aortic pressure with vasoactive drugs. Aortic pressure is increased with infusion of vasoconstrictor phenylephrine (PE) and decreased with infusion of vasodilator sodium nitroprusside (SNP). Aortic pressure plateaus 1 minute after the start of the drug infusion. M-mode of the aortic diameter is recorded at the plateau. (A) shows the rise in aortic pressure with 360 µg/kg/min PE infusion. (B) shows the decrease in aortic pressure with 240 µg/kg/min SNP infusion. The time the infusion is begun and the time the M-mode is recorded are labeled on the traces.

Figure reprinted with permission from Kuo MM, Barodka V, Abraham TP, Steppan J, Shoukas AA, Butlin M, et al. Measuring ascending aortic stiffness *in vivo* in mice using ultrasound. J Vis Exp 2014; e52200.

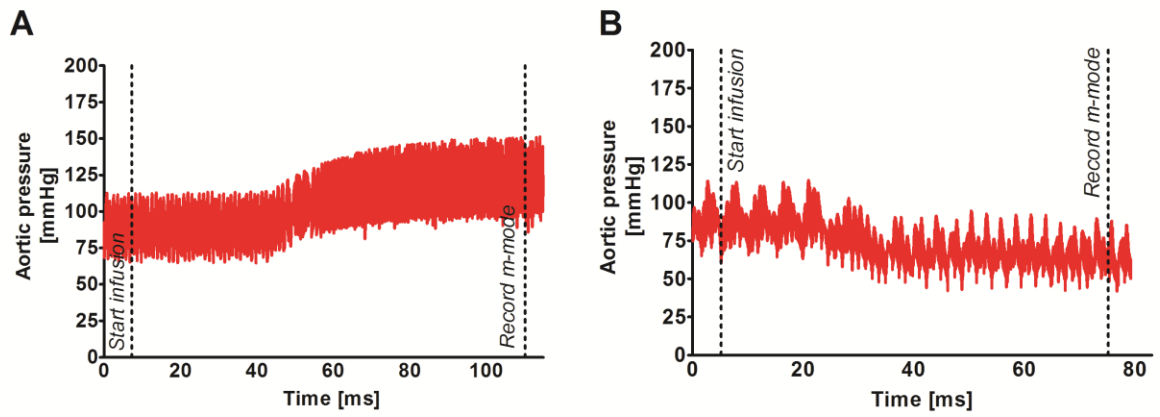

Figure 1.2.5: Changing aortic pressure incrementally. Aortic pressure is changed incrementally by the dose of drug infused. Drug dose is modulated by the infusion rate. All doses are in µg/kg/min.

Figure reprinted with permission from Kuo MM, Barodka V, Abraham TP, Steppan J, Shoukas AA, Butlin M, et al. Measuring ascending aortic stiffness *in vivo* in mice using ultrasound. J Vis Exp 2014; e52200.

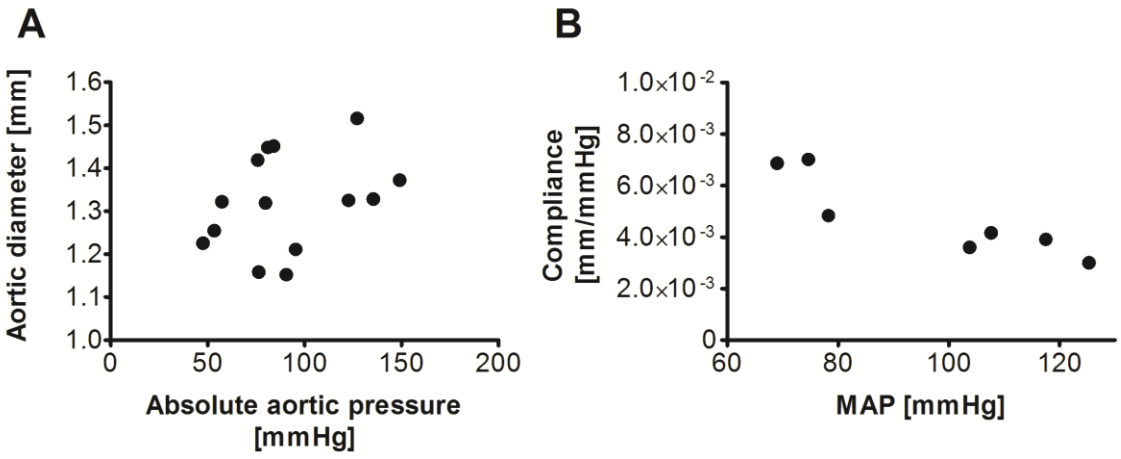

Figure 1.2.6: Diameter vs. pressure and compliance vs. mean aortic pressure plots. Aortic diameter can be plotted against its corresponding aortic pressure to show the pressure-diameter relationship (A). Compliance can be calculated for each pressure increment and plotted against the mean aortic pressure (MAP) to show the pressure dependency of aortic stiffness (B).

Figure reprinted with permission from Kuo MM, Barodka V, Abraham TP, Steppan J, Shoukas AA, Butlin M, et al. Measuring ascending aortic stiffness *in vivo* in mice using ultrasound. J Vis Exp 2014; e52200.

CHAPTER 2: EARLY EFFECTS OF IONIZING RADIATION ON CORONARY ARTERY FUNCTION

2.1. INTRODUCTION

The prevalence of coronary artery disease after ionizing radiation exposure is well-documented in the epidemiological literature. Increased incidence of coronary event has been reported in populations exposed to high doses, particularly breast cancer and Hodgkin's lymphoma patients who received radiotherapy *[27,28]*, as well as populations exposed to low doses, notably Japanese atomic bomb survivors *[29]*. These studies showed that the risk of heart disease increases proportionally with radiation dose with either no apparent *[27]* or a very low threshold of 0.5 Gy *[29]*. The mechanisms initiated by ionizing radiation exposure to result in the development of coronary artery disease are still not well understood. Moreover, whether these mechanisms are similar to those initiated by traditional risk factors of cardiovascular diseases, such as aging, is not firmly established.

The literature presents some indication that the development of radiation-induced coronary artery disease is similar to the progression of coronary artery disease. Coronary artery disease is associated with increased aortic stiffness *[13]*, hypertension *[30]* and diminished coronary vasodilatory function *[1]*, including endothelial-mediated vasodilation *[31,32]*. These markers of coronary artery disease have also been documented in exposed populations. Greater arterial stiffness was reported in Hodgkin's lymphoma patients who received radiotherapy *[33]*. The hypertensive effect of aging was accentuated in Japanese atomic bomb survivors *[34]*. In breast cancer patients who received radiotherapy treatment, vessels in the field of radiation had

attenuated endothelial-mediated vasorelaxation whereas non-exposed vessels had intact vasodilatory responses *[35]*.

On the cellular level, coronary artery disease, and cardiovascular diseases in general, is associated with excess reactive oxygen species (ROS) production in the endothelium. ROS scavenges vasodilatory nitric oxide (NO), decreasing NO bioavailability, and leading to oxidative stress and endothelial dysfunction *[36,37]*. Enzymatic sources of ROS associated with the development of coronary artery disease have also been reported in radiation-induced vascular dysfunction. Patients with coronary artery disease were shown to have augmented activity of xanthine oxidase (XO) and increasing XO activity corresponded with decreasing endothelial-mediated vasodilation *[38]*. Ionizing radiation exposure was demonstrated to lead to enhanced XO activity in large conduit arteries of exposed rats, resulting in elevated ROS level and impaired endothelial function *[39,40]*. Moreover, counteracting augmented ROS production by inhibiting the enzymatic source has been demonstrated to improve vascular function in both coronary artery disease patients and large conduit arteries of irradiated rats. Acute intravenous administration of XO inhibitor oxypurinol attenuated acetylcholine-induced coronary vasoconstriction and increased coronary blood flow in coronary artery disease patients who displayed coronary endothelial dysfunction *[41]*. Acute incubation of aortas from irradiated rats with oxypurinol restored endothelial-dependent vasorelaxation. Dietary supplementation of oxypurinol also prevented radiation-induced endothelial dysfunction in aortas from exposed rats *[39,40]*. These studies support excess ROS as the common element between coronary artery disease and radiation-induced vascular dysfunction.

Animal studies on vascular effects of radiation exposure have only been conducted in large conduit arteries. None to date have been conducted in the coronary arteries. We

hypothesize that exposure to ionizing radiation induces the same mechanistic events that promote the development of coronary artery disease: radiation exposure elevates ROS level in the coronary vasculature, leading to impaired coronary endothelial function. We investigate coronary vasorelaxation response in *vivo* one week after a single exposure to 5 Gy ionizing radiation in a rat model. We simultaneously measure the systemic parameters that influence coronary function: diastolic blood pressure, heart rate and contractility, and aortic stiffness. We further examine coronary vasodilatory response *ex vivo* to investigate endothelial function. We then consider the role of ROS and investigate the use of ROS scavengers and xanthine oxidase inhibitors in improving coronary function after radiation exposure.

2.2. METHODS

2.2.1. Animals and radiation procedure

All animal use was approved by the Animal Care and Use Committee at Johns Hopkins University. Male, 250-300 g Sprague-Dawley rats (Harlan) were exposed to a single dose of 5 Gy whole-body gamma radiation using a cesium-137 source (MSD Nordion Gammacell 40) with dose rate 0.91 Gy/min. All *in vivo* and *ex vivo* coronary vasoreactivity experiments were performed at 1 week after radiation exposure. *In vivo* and *ex vivo* aortic stiffness measurements were conducted 1 day and 2 weeks after exposure.

2.2.2. High-resolution transthoracic echocardiography

Coronary flow velocity and aortic diameter were measured *in vivo* by ultrasound using a 15 MHz transducer (Visual Sonics). The transducer was mounted on a stand (Visual Sonics) to record images and Doppler signals from the same location for the duration of the experiment.

Rats were anesthetized with 1.5% isoflurane. Chest hair was removed by shaving followed by application of depilatory cream. The animal was secured onto a heated platform to monitor ECG, heart rate, and body temperature. Drugs were administered intravenously through a 27G winged infusion set (Terumo) inserted into the lateral tail vein. Dose of drug was controlled with a syringe pump by adjusting infusion rate (Harvard Apparatus). All drugs were dissolved in 0.9% saline.

2.2.3. In vivo coronary vasoreactivity

The left main coronary artery was visualized from a long axis view by color Doppler flow, as described previously *[2]*. Flow velocity profile of the coronary artery was captured by pulse wave velocity. The difference in angle between blood flow and ultrasound beam was accounted for with angle correction on the Vevo mainframe. Agonist-mediated vasorelaxation response was examined by infusing vasodilator adenosine triphosphate (ATP, Sigma) at 20, 40, 80, and 160 μg/kg/min for 1 minute per dose. Increasing diameter corresponded with increasing flow velocity. Peak diastolic flow velocity of three cardiac cycles was measured for data analysis.

Metabolic demand-mediated vasorelaxation response was characterized by infusing dobutamine (Dob, Hospira) at 5, 10, 20, and 30 ug/kg/min for 2 minutes per dose. Dobutamine challenge was performed twice. Flow velocity was recorded the first round. M-mode images of the left ventricle were recorded the second round for left ventricular diameter measurement.

Peak diastolic flow velocities of three cardiac cycles were measured for vasorelaxation analysis. Cardiac contractility was measured as fractional shortening calculated from the end-

diastolic and end-systolic diameters of three cardiac cycles. Measurements were done on the Vevo 2100 mainframe.

2.2.4. In vivo aortic pressure-diameter relationship

In vivo stiffness of the ascending aorta was measured as described in Chapter 1.2. Ascending thoracic aorta was visualized from a long axis view. Aortic diameter was recorded above the aortic valve by M-mode. Blood pressure was increased step-wise by infusing 100 μg/mL phenylephrine (PE, Sigma) at 50, 100, and 200 μL/min at 30 seconds per dose. After return to baseline, blood pressure was decreased step-wise by infusing 100 μg/mL of sodium nitroprusside (SNP, Sigma) at 50, 100, and 200 μL/min at 30 seconds per dose. Diastolic and systolic diameters and corresponding blood pressures of three cardiac cycles were measured from the M-mode images for each PE and SNP dose.

Ascending aorta compliance was calculated as described for *ex vivo* preparations *[19]*. For a constant vessel length, volume within the vessel is proportional to the diameter squared. The equation for vessel compliance therefore becomes $C = \Delta V / \Delta P = \Delta D^2 / \Delta P$, where C is compliance, ΔV is change in volume, ΔP is change in pressure, and ΔD^2 is change in squared diameter. Aortic diameter squared was plotted against the corresponding blood pressure and a line was fitted to the resulting plot using a linear least squares-fit algorithm (GraphPad). The slope of the fitted line was used as a measure of aortic compliance.

2.2.5. Invasive aortic blood pressure measurement

A 1.2F solid-state catheter (Transonic) was inserted into the right femoral artery and advanced into the abdominal aorta. Signal output from the pressure control unit was split with a

BNC splitter. One output was connected to the Powerlab and LabChart data acquisition system (AD Instruments) for real-time display of blood pressure. The second output was connected to the high-resolution ultrasound system (Vevo 2100, Visual Sonic) for simultaneous recording of blood pressure with ultrasound measurements. Aortic pressure was measured in a separate set of animals for the coronary vasoreactivity challenges and simultaneously for the *in vivo* aortic stiffness measurements.

2.2.6. Aortic tensile testing

Following *in vivo* stiffness measurement, rat was euthanized by exsanguination and the aorta was harvested and cleaned. Ring sections were cut from the ascending aorta. Aortic rings were imaged and ring length and inner and outer diameters were measured with ImageJ (National Institute of Health). The sample was mounted onto two pins of a tissue puller (Danish Myo Technology). The ring was pulled apart to material failure and the force generated by displacement was recorded on the system's data acquisition software. Displacement was converted to strain by normalizing to the inner diameter of the ring. Force was converted to stress by dividing measured force by cross-sectional area of the vessel wall, calculated as the product of wall thickness and ring length. Because the recorded strain values were different for each sample, the stress-strain plot of each sample was fitted with an exponential curve on Prism (GraphPad). A new set of stress values was then calculated from the fitted equation using a set of strain values that was used for every sample.

2.2.7. Ex vivo coronary vasoreactivity

Rats were euthanized by isoflurane overdose and left main and descending coronary artery was dissected and sectioned into ~1mm rings. Precise vessel section length was measured and vessel sections were mounted onto a wire myograph (DMT). Vessels were bathed in 95/5% O2/CO2 oxygenated Krebs physiological solution containing in [mM] 118 NaClm 4.7 KCl, 25.0 NaHCO3, 1.2 MgSO4, 1.1 KH2PO4, 11 glucose, and 2.5 CaCl2-2H2O maintained at 37C. Vessels were equilibrated for 30 minutes and then stretched in 0.3 mN increments to the tension equivalent to 50 mmHg (6.7 kPa), as determined by the DMT normalization module for LabChart. After stretching, vessels were equilibrated for 15 minutes, and then subjected to two rounds of 60mM KCl bolus injection into the bath.

Rings were pre-constricted with 10^{-6} M prostaglandin F2α (Cayman Chemicals) or $10^{-6.5}$ M prostaglandin H2 analog U46619 (Cayman Chemicals). Cumulative doses of acetylcholine (Ach, Sigma Aldrich) and sodium nitroprusside (SNP, Sigma Aldrich) were added to evaluate endothelial-dependent and –independent vasorelaxation. Relaxation tensions were normalized to pre-constriction tension for data analysis.

In a separate set of experiments, coronary rings were pre-constricted with U46619 and once a steady pre-constriction was reached, further constricted with the addition of 100 μM of nitric oxide synthase inhibitor L-NG-nitroarginine methyl ester (L-NAME, Cayman Chemicals). Increase in constriction tension was measured as the percent increase in coronary tone after the addition of L-NAME compared to the U46619-induced pre-constriction tension.

2.2.8. In vitro measurement of total reactive oxygen species (ROS) content

Left main and descending coronary arteries were harvested and snap frozen at 2 weeks post-irradiation. Frozen samples were homogenized in radioimmunoprecipitation assay (RIPA,

Upstate) with protease inhibitor buffer. Total reactive oxygen species (ROS) was measured in the homogenate with the OxiSelect *In Vitro* ROS/RNS Assay Kit (Cell Biolabs, Inc.), following the manufacturer's directions. Homogenate was incubated with 100 μM and 500 μM superoxide dismutase mimetic, manganese (III) tetrakis (4-benzoic acid) porphyrin (MnTBAP, CalBiochem) or 1mM oxypurinol (Oxp, Sigma). ROS content was measured in terms of ROS production rate and normalized to the amount of protein. Data is expressed as relative fluorescent unit (RFU)/min/mg protein.

2.2.9. In vivo testing of ROS and its enzymatic sources

Rats were administered an intravenous bolus infusion of 1 mg/kg MnTBAP, 10 mg/kg oxypurinol, or 10 mg/kg of an alternate XO inhibitor, allopurinol (Allo, Sigma). Basal and ATP-induced increase in flow velocity measurements were taken two minutes after infusion for MnTBAP treatment and 15 minutes after infusion for oxypurinol and allopurinol treatments.

2.2.10. Statistical analysis

Statistical significance was determined by Student's t-test or two-way analysis of variance with Bonferroni post-test using Prism (GraphPad). Data are reported as mean±SEM.

2.3. RESULTS

2.3.1. In vivo coronary vasoreactivity

We first characterized coronary vasodilatory function after radiation exposure. At one week post-irradiation, ATP-induced increase in flow velocity was diminished in 5 Gy rats ($p<0.001$, Fig. 2.1A). Metabolic demand-induced increase in flow velocity was also attenuated in

5 Gy rats ($p<0.001$, Fig. 2.1B). Flow velocity at dobutamine dose 30 μg/kg/min was 957.3±18.2 mm/s in 0 Gy compared 815.7±56.3 mm/s in 5 Gy, $p<0.01$. Corresponding diastolic aortic pressure was also significantly reduced for both ATP ($p<0.001$, Fig. 2.1C) and dobutamine responses ($p<0.001$, Fig. 2.1D).

We next considered the influence of cardiac function on coronary flow through heart rate and contractility. Heart rate was lower in 5 Gy rats for both ATP ($p<0.001$, Fig. 2.2A) and dobutamine responses ($p<0.001$, Fig. 2.2B). Contractility response to dobutamine was enhanced in 5 Gy rats ($p<0.01$, Fig. 2.2C). Fractional shortening at 30 μg/kg/min dobutamine was 61.4±2.9% in 0 Gy compared to 76.2±1.7% in 5 Gy rats, $p<0.01$.

We further investigated if changes in aortic stiffness occurred with radiation exposure. *In vivo* ascending aortic stiffness in 5 Gy rats increased 1 day after exposure and returned to 0 Gy level by 2 weeks post-exposure (Fig. 2.3A). 0 Gy compliance was 5.5±0.4 $x10^{-2}$ mm^2/mmHg and 5 Gy ascending aortic compliance at 1 day was 4.0±0.5 $x10^{-2}$ mm^2/mmHg, $p=0.020$. At 2 weeks, 5 Gy ascending aortic compliance was 5.6±0.4 $x10^{-2}$ mm^2/mmHg, $p=0.016$ compared to 1 day stiffness. *Ex vivo* measurement of ascending aortic stiffness showed no changes in stiffness at 1 day or 2 weeks post-radiation exposure (Fig. 2.3B).

2.3.2. Ex vivo coronary vasoreactivity

To determine if decreased coronary tone observed *in vivo* was due to impaired coronary vasodilatory function, we examined coronary vasoreactivity *ex vivo* by wire myography. No change in endothelial-dependent relaxation was observed one week after radiation exposure (Fig. 2.4A). However, endothelial-independent relaxation was enhanced ($p<0.05$, Fig. 2.4B). Pre-

constriction tone normalized to vessel length and L-NAME-induced increase in pre-constriction tone were not different between cohorts (Fig. 2.4C).

2.3.3. Coronary ROS level and NO bioavailability

We next considered NO availability in the coronary artery after radiation exposure with *in vitro* ROS measurement and basal coronary flow. Coronary ROS level 2 weeks post-exposure was greater in coronary arteries of 5 Gy rats than of 0 Gy rats: ROS amount was 1999.7±347.3 ROS/mg protein in 0 Gy compared to 4802.6±1141.6 ROS/mg protein in 5 Gy rats, $p = 0.047$ (Fig. 2.5A). Incubation with MnTBAP reduced ROS amount in both 0 Gy and 5 Gy groups. ROS abundance was not different between cohorts after incubation with 100 μM and 500 μM MnTBAP. 500 μM MnTBAP significantly reduced ROS in the 5 Gy coronary arteries: ROS content was 1471.7±183.0 ROS/mg protein with 500 μM MnTBAP compared to 4802.6±1141.6 ROS/mg protein in untreated vessels, $p=0.026$. Incubation with 1 mM oxypurinol (Oxy) did not change ROS content in the 0 Gy group but reduced ROS in the 5 Gy group to 0 Gy level ($p = 0.089$): ROS amount was 2632.3±282.2 ROS/mg protein in Oxy-incubated 5 Gy coronary tissue compared to 2699.3±511.5 ROS/mg protein in Oxy-incubated 0 Gy tissue.

NO bioavailability was further examined *in vivo* by measuring changes in basal coronary flow with infusion of ROS scavengers and inhibitors (Fig. 2.5B). Basal coronary flow velocity was significantly lower in 5 Gy rats than in 0 Gy rats: flow velocity was 356.8±13.3 mm/s in 5 Gy compared to 463.6±13.2 mm/s in 0 Gy, $p=0.0001$. MnTBAP infusion increased basal flow velocity in 5 Gy rats to the level of 0 Gy rats: flow velocity was 507.0±23.3 mm/s in MnTBAP-infused 5 Gy animals compared to 356.8±13.3 mm/s in untreated 5 Gy animals, $p <0.0001$. Xanthine oxidase inhibitor allopurinol (Allo) partially restored baseline flow: 411.3±18.17 mm/s

in Allo-treated 5 Gy rats compared to 356.8±13.34 mm/s in untreated 5 Gy rats, p = 0.044. Oxypurinol also increased basal flow velocity in 5 Gy to a similar extent as allopurinol, although the difference was not statistically significant: 404.0±42.2 mm/s with oxypurinol treatment compared to 356.8±13.3 mm/s without treatment in 5 Gy, p=0.085.

We sought to determine if *in vivo* coronary vasodilatory response was similarly improved. Although acute XO inhibition improved resting tone, it did not improve vasodilatory response. ATP-mediated vasorelaxation with allopurinol (Fig. 2.6A) and oxypurinol (Fig. 2.6B) treated 5 Gy rats were not statistically different than untreated 5 Gy rats.

2.4. DISCUSSION

This study is the first to investigate the effects of radiation exposure in the coronary artery. Our data show that single whole-body exposure to 5 Gy ionizing radiation reduces coronary flow in vivo. The reduced coronary flow is attributed to a combination of decreased diastolic aortic pressure and excess scavenging of NO by ROS. Endothelial-mediated vasodilatory function and eNOS activity, however, remain intact after radiation exposure. The data support that elevated ROS is the initial sign of radiation injury and precedes endothelial dysfunction that lead to later development of coronary artery disease.

The reduced flow velocity observed in vivo in 5 Gy rats could arise from increased coronary tone and impaired vasodilatory capacity or reduced coronary perfusion pressure. We first considered the influences of perfusion pressure. Examination of coronary perfusion pressure through aortic diastolic pressure showed that diastolic pressure was reduced in 5 Gy rats. We next investigated whether radiation exposure altered the systemic parameters that influence diastolic pressure, namely heart rate and aortic stiffness. We found that heart rate was also lower

in 5 Gy rats. The restoration of in vivo aortic stiffness from one day post-irradiation to two weeks post-irradiation support that stiffness at one week was not increased enough to appreciably influence diastolic pressure. Tensile testing data further showed that tensile properties of the aortic wall did not change over the two week period, indicating that wall remodeling and changes to aortic wall content did not occur within two weeks after radiation exposure. Taken together, the data show that the decreased flow velocity observed in vivo can be attributed to reduced diastolic pressure. Reduced diastolic pressure appears to be predominantly due to changes in heart rate and not aortic stiffness, suggesting that radiation has direct effects on heart function.

We next considered if the reduced in vivo coronary flow was also the result of impaired vasodilatory function. Endothelial-mediated vasorelaxation response was not different between 0 Gy and 5 Gy rats. However, endothelial-independent vasorelaxation response to NO donor SNP was enhanced, supporting that coronary arteries of 5 Gy rats exhibited increased sensitivity to NO. If production of NO was reduced, the enhanced NO sensitivity could compensate to some extent for the decrease in NO, resulting in intact endothelial-mediated vasorelaxation. We determined if eNOS activity and therefore NO production was impaired by evaluating U46619 pre-constriction tone and L-NAME-induced increase in pre-constriction tone. Pre-constriction tone is a balance between the vasoconstrictive effects of the pre-constricting agent and the vasodilatory mediators that are produced basally by the endothelium. Reduction of basal production of vasodilatory mediators, including NO, results in increased pre-constriction tone and has been previously shown experimentally with NO production cessation by L-NAME *[42]*. Addition of L-NAME after the coronary artery reaches a steady pre-constriction tone would similarly increase pre-constriction tension. Our data showed that U46619 pre-constriction tone

when normalized to vessel length was not different between 0 Gy and 5 Gy animals, supporting that basal production of vasodilatory mediators was not impaired. This finding is further corroborated by the similar L-NAME-induced percent increase in pre-constriction tone between the cohorts.

While the reduced coronary flow observed in vivo was not associated with impaired coronary endothelial-mediated vasodilatory function or eNOS activity, it could potentially be explained by reduced NO bioavailability. *In vitro* measurement of ROS level in the coronary tissue showed elevated superoxide level, supporting reduced NO bioavailability from excess ROS-mediated scavenging. Because NO is the primary vasoactive mediator of baseline coronary tone *[43,44]*, basal coronary flow can also be used as a measure of NO bioavailability. Changes in in vivo baseline coronary flow with administration of ROS scavengers and ROS producer inhibitors were consistent with in vitro ROS measurements. 5 Gy rats exhibited reduced basal coronary flow, which supports diminished NO bioavailability, as well as elevated superoxide content in vitro, which supports excess scavenging of NO. Bolus infusion of MnTBAP raised coronary flow, as in vitro incubation with MnTBAP reduced coronary ROS. Acute administration of xanthine oxidase inhibitors oxypurinol and allopurinol partially restored baseline coronary flow in 5 Gy rats, consistent with the partial reduction of ROS content in vitro with oxypurinol incubation. Together, the data support that ROS content in the coronary artery is increased after radiation exposure and that NO bioavailability is reduced because of excess ROS scavenging.

The findings of this study are particularly intriguing when considering the long latency period between diagnosis of coronary artery disease and radiation exposure. The mean time of diagnosis of coronary artery disease symptoms in cancer patients who underwent radiation

therapy is 7 years after treatment *[45]*. Furthermore, epidemiological and patient studies investigating vascular effects of radiation exposure are conducted several years after the patients underwent treatment. The presence of physiological dysfunction years after radiation exposure could indicate that initial radiation exposure causes direct endothelial injury and that vascular damage is sustained. Or, as the long latency period suggests and this study supports, radiation-induced vascular dysfunction is progressive. Radiation-associated cardiovascular disease is not due to direct cellular damage from the radiation exposure, but, appears to be analogous to aging-associated vascular diseases. Vascular aging is characterized by endothelial dysfunction that is initiated by elevated superoxide production and subsequent scavenging of NO *[46]*. Our data support that radiation-associated coronary artery disease is similarly initiated by augmented superoxide release which leads to excess NO scavenging and eventually results in coronary endothelial dysfunction characteristic of coronary artery disease.

Although inhibition of xanthine oxidase partially restored baseline flow in 5 Gy rats, it did not restore coronary flow. In the patient study that showed improvement in coronary function with acute oxypurinol treatment, endothelial-mediated vasorelaxation was improved with treatment in coronary artery disease patients who exhibited impaired coronary endothelial function *[41]*. The treatment had no effect in patients who had intact coronary endothelial function. Endothelial-mediated vasorelaxation and eNOS activity were intact in 5 Gy rats, supporting that endothelial function was preserved. Xanthine oxidase inhibitor treatment therefore had no effect in 5 Gy rats because these rats did not display impaired coronary endothelial function.

Phenotypical changes in the coronary artery after radiation exposure appear similar to aging. However, cardiac function after radiation exposure does not. Cardiac function diminishes

with age and is associated with reduced β-adrenergic responsiveness arising from a combination of decreased expression of β-adrenergic receptors, decreased agonist binding, and dysregulated downstream signal transduction *[47]*. The reduced heart rate observed in this study could therefore be due to a reduction in β-adrenergic receptor expression or impaired receptor function. However, rabbits exposed to 5 Gy whole-body X-ray radiation only exhibited a slight decrease in expression and binding affinity of β-adrenergic receptors at 3 days that tended towards non-irradiated values by 7 days *[48]*. The reduced heart rate observed in this study therefore does not appear to be a result of reduced receptor expression or binding affinity. Dysregulated downstream signaling could also result in decreased heart rate. However, contractility data showed enhanced contractility in 5 Gy rats, suggesting enhanced responsiveness of β-adrenergic signaling. Changes in cardiac function therefore appear to occur by mechanisms different than those that occur with aging.

The aortic stiffness data reported in this study conflicts with a previous study by Soucy et al. *[39]* that reported an increase in aortic stiffness one day after exposure to 5 Gy gamma radiation that remained sustained at 2 weeks post-irradiation. The radiation source and rat strain used in this study were the same as the Soucy et al. study. Discrepancy in findings could be attributed to different measurement methodologies. Soucy et al. measured aortic stiffness by pulse wave velocity while this study measured aortic stiffness from the pressure-diameter relationship and by tensile testing. More likely, however, the discrepancy is due to the difference in age of the rats at the time of radiation exposure. Rats used in this study were 2 months old while the rats used in the Soucy et al. study were 3-4 months. Epidemiological studies have shown that age at radiation exposure influences likelihood of future cardiovascular event. When the risk of major coronary event in breast cancer patients who had received radiotherapy was

stratified by age, risk of major coronary event was dramatically less in women age 20-39 at the time of diagnosis than in women 40 and above *[27]*. Although the confidence interval was very wide for this age group, the influence of age at the time of radiotherapy on the risk of future cardiovascular events has been reported in other studies. The effect of radiation exposure on aortic and carotid artery stiffness in Hodgkin's lymphoma patients who had undergone radiotherapy was more pronounced in patients who were treated at age 40 and above *[33]*. 2-month old rats were used in this study because the left coronary artery was easier to locate than in than 3-month old rats. This discrepancy in findings highlights the importance of age at the time of radiation exposure and support the epidemiological literature that suggests a younger vasculature is more adept at handling radiation injury.

2.5. FIGURES

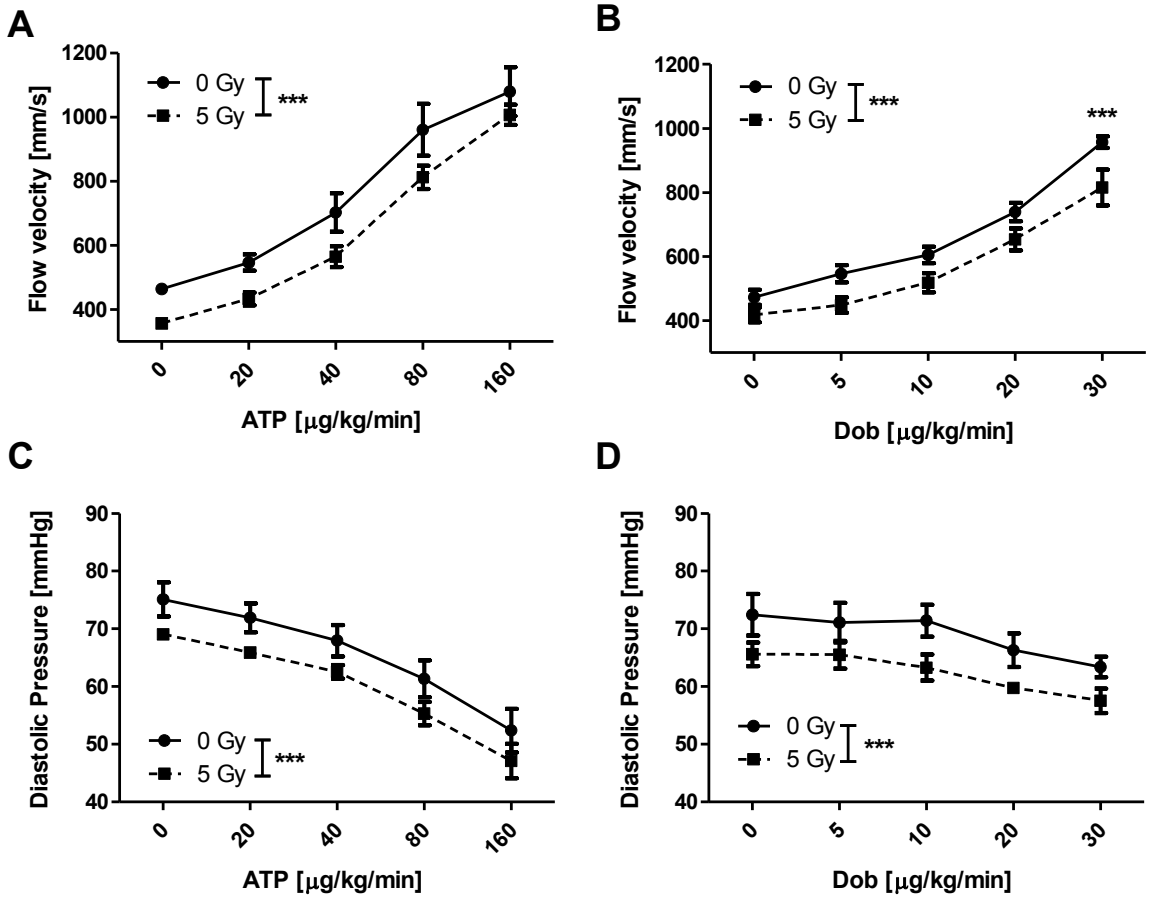

Figure 2.1. Coronary vasoreactivity *in vivo*. Coronary vasodilatory function was evaluated *in vivo* using high-resolution ultrasound. Vasorelaxation function was assessed in terms of agonist-mediated vasorelaxation with vasodilator adenosine triphosphate (ATP) and myocardial demand-mediated vasorelaxation with β-adrenergic receptor agonist dobutamine (Dob). Increase in coronary artery diameter was reflected in an increase in coronary flow velocity. 5 Gy rats exhibited attenuated ATP-mediated (A) and metabolic demand-mediated (B) vasorelaxation response, ***$p<0.001$. Diastolic aortic pressure was used to evaluate coronary perfusion pressure. 5 Gy rats exhibited reduced diastolic pressure during the ATP (C) and dobutamine (D) challenges. Drug doses are in units of μg/kg/min.

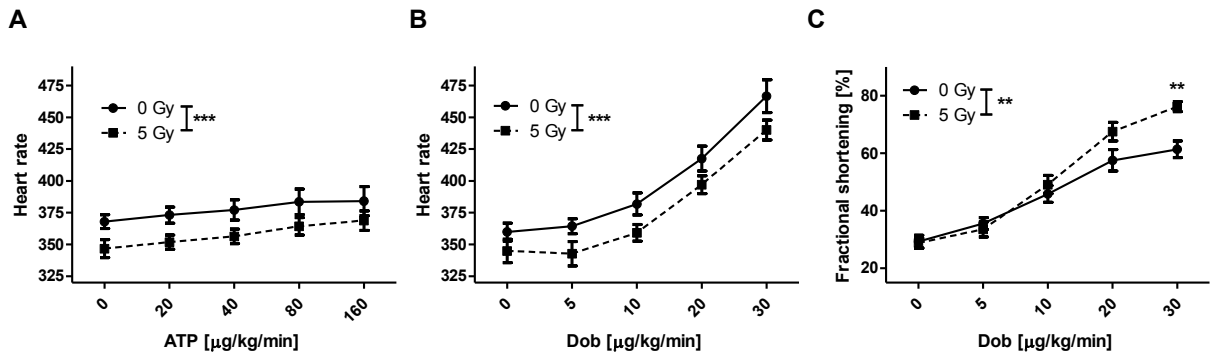

Figure 2.2. Cardiac parameters that influence coronary flow. Heart rate and cardiac contractility were measured to determine if changes in cardiac function could account for the decreased coronary flow. 5 Gy rats exhibited reduced heart rate during ATP (A) and dobutamine (Dob) (B) challenges, ***$p<0.001$. Cardiac contractility, measured as fractional shortening (C), was enhanced in 5 Gy rats, **$p<0.01$. Drug doses are in units of µg/kg/min.

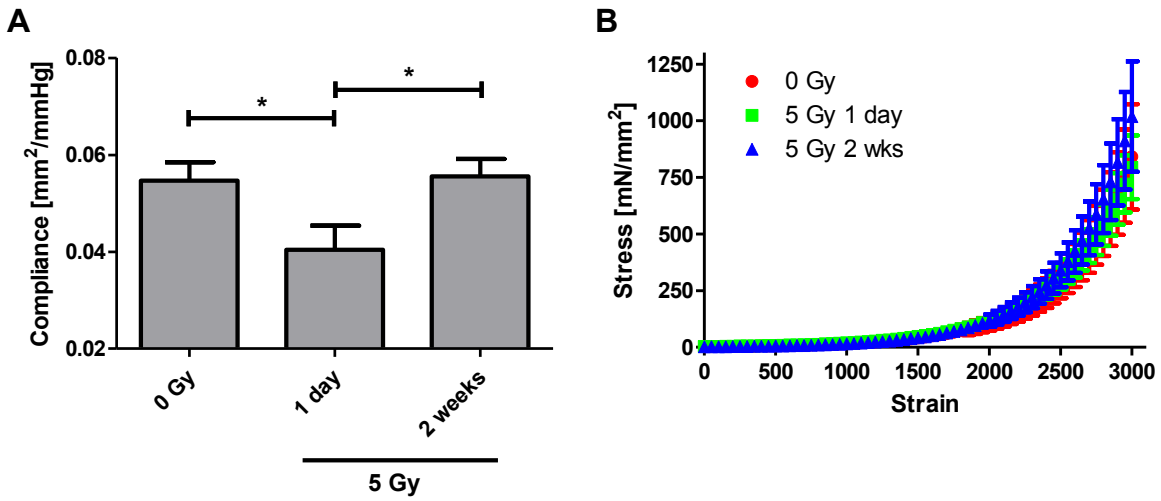

Figure 2.3. *In vivo* and *ex vivo* ascending aorta stiffness. Aortic stiffness was measured to determine if ionizing radiation induced changes in stiffness that would in turn influence coronary perfusion pressure and coronary flow. Stiffness of the ascending aorta was determined *in vivo* from its pressure-diameter relationship measured by ultrasound imaging and invasive measurement of aortic pressure. Aortic stiffness was measured *ex vivo* by tensile testing. 5 Gy rats exhibited decreased *in vivo* compliance, indicating increased stiffness, at 1 day post-irradiation that returned to 0 Gy value by 2 weeks post-irradiation, *$p<0.05$ (A). *Ex vivo* stiffness measured by tensile testing showed no difference between 0 Gy and 5 Gy aortas over the 2 week period following radiation exposure (B).

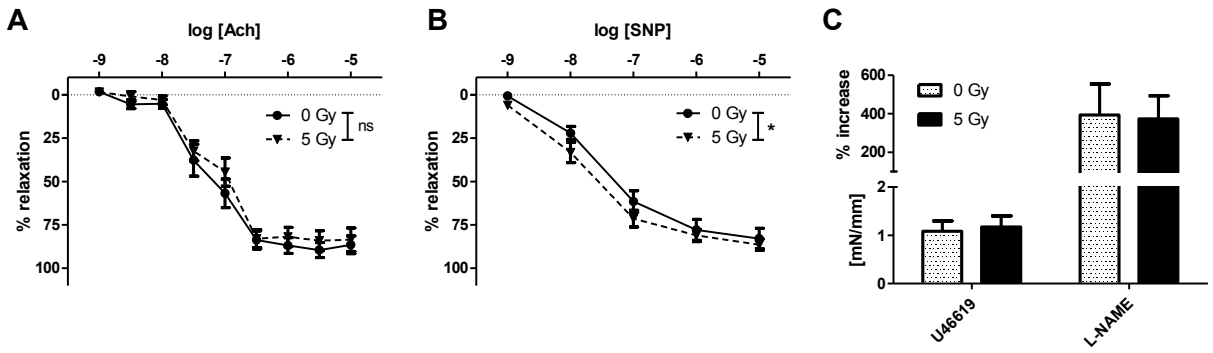

Figure 2.4. Coronary vasoreactivity *ex vivo*. Coronary endothelial function was measured *ex vivo* by wire myography. 5 Gy rats exhibited similar endothelial-mediated vasorelaxation response as 0 Gy rats (A). However, 5 Gy rats also displayed enhanced endothelial-independent nitric oxide-mediated vasorelaxation response (B), *$p<0.01$. eNOS activity was evaluated by $10^{-6.5}$ M U46619 pre-constriction tone normalized to vessel ring length and 100 µM NOS inhibitor L-NAME induced percent increase in pre-constriction tone. Both pre-constriction tone and L-NAME enhanced tone were not different between cohorts (C).

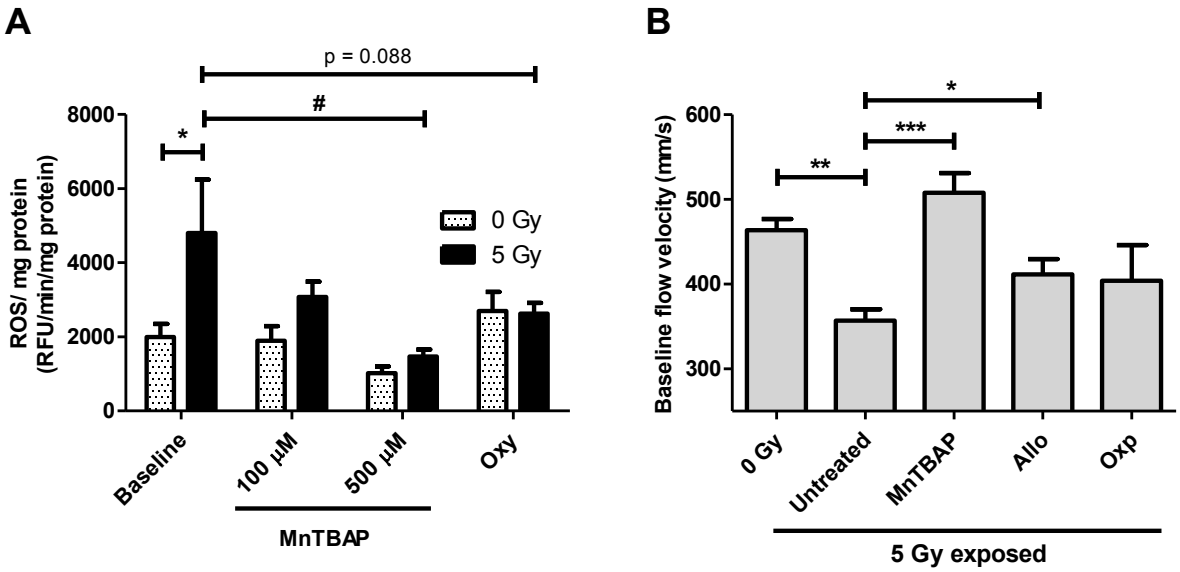

Figure 2.5. *In vitro* and *in vivo* assessment of NO bioavailability. ROS content and *in vivo* basal coronary flow were measured to evaluate NO bioavailability. *In vitro* measurement of ROS content showed that coronary arteries from 5 Gy rats had significantly higher ROS content than coronary arteries from 0 Gy rats (A). Incubation with 500 µM superoxide scavenger MnTBAP, reduced ROS content in 5 Gy arteries significantly, #$p<0.05$ between 5 Gy and 5 Gy + 500 µM MnTBAP. Inhibition of ROS production by xanthine oxidase inhibition with 1 mM oxypurinol (Oxy) partially reduced ROS content in 5 Gy coronary arteries. *In vivo* assessment of NO bioavailability by baseline flow velocity showed that 5 Gy rats had significantly reduced baseline flow velocity compared to 0 Gy rats (B). Acute infusion of 1 mg/kg MnTBAP dramatically increased basal flow in 5 Gy rats whereas acute infusion of xanthine oxidase inhibitors allopurinol (Allo) and Oxy at 10 mg/kg partially restored basal flow. *$p<0.05$, **$p<0.01$, ***$p<0.001$.

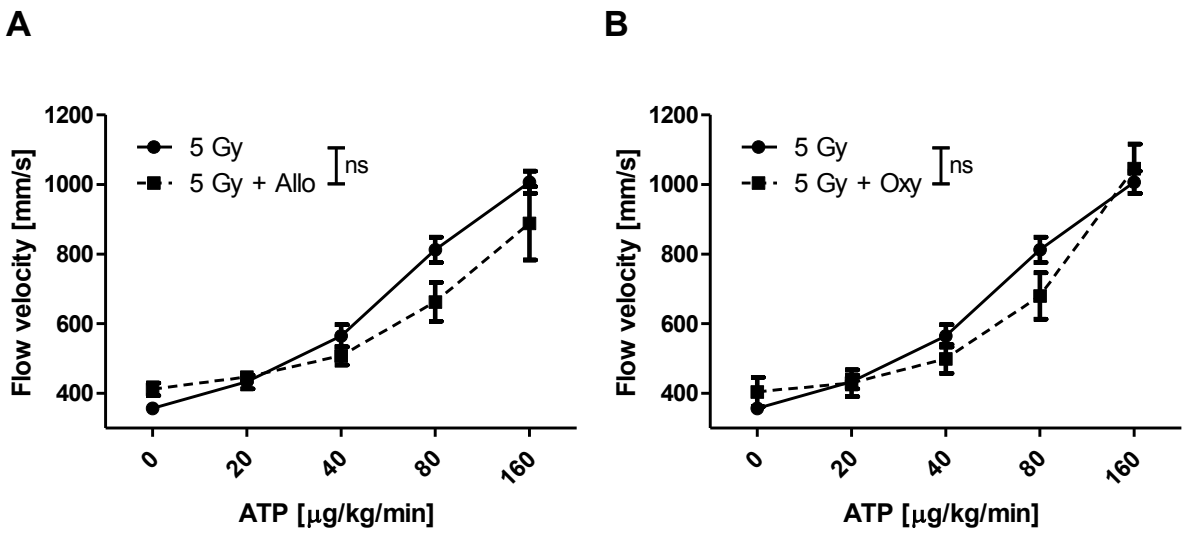

Figure 2.6. Effectiveness of ROS production inhibition on restoring *in vivo* coronary vasodilatory function. Xanthine oxidase inhibitors were administered to determine if xanthine oxidase inhibition could improve coronary flow in 5 Gy rats. Neither 10 mg/kg allopurinol (A) or 10 mg/kg oxypurinol (B) treatment restored coronary flow.

CHAPTER 3: MPST AND NOT CSE IS THE PRIMARY REGULATOR OF HYDROGEN SULFIDE PRODUCTION AND FUNCTION IN THE CORONARY ARTERY

3.1. INTRODUCTION

Coronary tone is regulated by the endothelium predominantly through vasodilatory mediators nitric oxide (NO) and endothelial-derived hyperpolarizing factors (EDHFs). NO is produced by endothelial nitric oxide synthase (eNOS) and has been demonstrated to regulate resting coronary tone *[49,50]* and metabolic demand-mediated vasodilation *[51]*. Of the EDHFs, hydrogen peroxide (H_2O_2) has been widely researched. H_2O_2 has similarly been shown to be involved in coronary autoregulation *[52]*, metabolic demand-mediated vasodilation *[53]*, and flow-mediated vasodilation *[54]*.

Another EDHF, hydrogen sulfide (H_2S), has recently emerged as another important gasotransmitter in the vasculature. H_2S is produced from L-cysteine by cystathionine gamma-lyase (CSE) and 3-mercaptopyruvate sulfurtransferase (MPST) *[55]*. CSE converts L-cysteine into H_2S with pyridoxal-5'-phosphate (PLP) as a cofactor. L-cysteine-dependent production of H_2S by MPST is a two-step reaction. First, cysteine aminotransferase converts L-cysteine along with α-ketoglutarate into 3-mercaptopyruvate (3-MP). MPST then converts 3-MP into H_2S *[56]*. CSE appears to have an important role in vascular tone regulation as mice lacking CSE are hypertensive and have attenuated endothelial-dependent vasodilation *[57]*.

Vasoactive effects of H_2S vary by vascular bed. In the mesenteric bed, H_2S is a vasodilator *[58]* while in the pulmonary bed, it is a vasoconstrictor *[59]*. In the aorta, the vasoactive effect of H_2S depends on dose *[60]*: H_2S is a vasoconstrictor at low doses and a

vasodilator at high doses. In the coronary vasculature, H_2S has been reported to be a vasodilator *[61]*, *[62]*. H_2S induces coronary vasodilation independent of the endothelium through 4-aminopyridine-sensitive K_v, BK_{Ca}, and K_{ATP} channels *[61-64]*. The role of CSE as a producer of endogenous H_2S has also been investigated, although conclusions regarding its contribution are inconsistent. Some studies support little contribution of CSE in coronary vasoregulation *[61,64]* while others support involvement *[62,63]*.

The role of MPST in coronary vasoregulation has not been examined. Moreover, the current literature on H_2S involvement in coronary vasoregulation lacks direct measurement of H_2S production in the coronary artery. In this study, we hypothesized that MPST is a source of endogenous H_2S in the coronary vasculature. We measured protein abundance of the two H_2S producing enzymes and measured *in vitro* H_2S production through both pathways. We next investigated the role of CSE-derived H_2S *in vivo* by measuring *in vivo* coronary vasorelaxation function in CSE inhibited and CSE knockout models. We then investigated the role of MPST-derived H_2S by characterizing the vasoactive effects of MPST substrate 3-MP in an *ex vivo* model.

3.2. METHODS

3.2.1. Animals

All animal use was approved by the Animal Care and Use Committee at Johns Hopkins University. *In vivo* coronary vasoreactivity experiments were performed in male, 12-18 week old CSE-deficient (CSE-/-) and B6129S (Jackson) wild-type mice. Male. 250-300g Sprague-Dawley rats (Harlan) were used for *ex vivo* experiments.

3.2.2. Cell culture

Human coronary artery (HCAECs, Lonza) and aortic endothelial cells (HAECs, Lonza) were cultured in endothelial basal medium supplemented with 5% fetal bovine serum, endothelial cell growth supplements, and penicillin/streptomycin (Lonza).

3.2.3. Protein expression

Protein expression was determined in human endothelial cells and rat vascular tissue by Western blot. Rat aorta and left coronary artery were harvested for analysis. Cells were lysed and tissue was homogenized in 1X radioimmunoprecipitation assay (RIPA) buffer (Upstate) containing protease inhibitors (Roche). Antibodies used were rabbit-polyclonal anti-MPST antibody (1:1000, Atlas Antibody), rabbit-polyclonal anti-CSE antibody (1:1000, ProteinTech) for human endothelial cells, and mouse-monoclonal anti-CSE antibody (1:1000, ProteinTech) for rat tissue. Mouse-polyclonal anti-GAPDH antibody was used as loading control (1:5000, Novus Biologicals). HRP-conjugated donkey anti-rabbit or sheep anti-mouse secondary antibody (1:5000, GE Healthcare) was used for detection. Blots were developed using SuperSignal West Pico Chemiluminescent Substrate (ThermoScientific). HAECs and rat aorta were used as positive controls.

3.2.4. In vitro amperometric H_2S measurement

Tissue H_2S production was measured by amperometry using the Apollo 4000 Free Radical Analyzer detector (WPI) and a 3-mm H_2S-selective electrode (WPI). Reactions were performed as previously described *[55]*. For MPST-mediated H_2S production, rat liver and coronary tissue samples were homogenized in cold 10X PBS buffer containing 1 mM

dithiothrietol (DTT; New England BioLabs) and protease inhibitor (Roche). Total reaction volume was 200 µL and total protein amount used was 300 µg for liver and 30 µg for coronary. Homogenate was incubated with MPST substrate 3-mercaptopyruvate (3-MP; Sigma) for 50 minutes at 37°C in 2 mL gas-tight vials (Fisher). Liver homogenate was incubated with the listed 3-MP concentrations. Coronary homogenate was incubated with 1 mM 3-MP. After 50 minutes of incubation, 200 µL of 10X PBS adjusted to pH 6.0 was added to the reaction to promote release of H_2S and to stop the reaction. The reaction was incubated at 37°C for another 10 minutes. 2 mL of headspace for liver samples and 3 mL of headspace for coronary samples was withdrawn from the gas-tight vial using a 10 mL syringe (BD) with a 22 G needle (BD) attached and injected into a scintillation vial containing 15 mL of 10X PBS (ThermoScientific) in which the amperometric probe was equilibrating. Amount of H_2S produced by the reaction was measured by the probe in units of pA. Data was recorded two minutes after the headspace gas was injected.

For CSE-mediated H_2S production, the tissue was homogenized in 10X PBS buffer containing protease inhibitor and incubated with 2 mM pyridoxal-5'-phosphate (PLP; Sigma) and L-cysteine (Sigma) *[65]*. Liver homogenate was incubated with listed L-cysteine concentrations. Coronary homogenate was incubated with 50 mM L-cysteine. Reaction incubation and measurement procedures were performed as described.

Experiments were done in triplicate. H_2S produced from liver homogenate was measured as the difference in amperometric signal between the liver homogenate incubated with the indicated substrate concentration and baseline signal of the homogenate with no substrate. H_2S produced by the coronary tissue was calculated as the difference between the substrate incubated with coronary homogenate and baseline signal of the substrate incubated with no protein

homogenate. A calibration curve for the amperometric probe was generated using H_2S donor sodium hydrosulfide (NaHS) and assuming that 1/3 of NaHS is in soluble H_2S form *[66]* to equate pA units to H_2S concentration.

3.2.5. In vitro fluorimetric H2S measurement

Fluorometric measurement of H_2S was performed using 7-Azido-4-Methylcoumarin (AzMC; Sigma). Reactions were carried out in 1X PBS (Invitrogen) in a black 96-well plate with total reaction volume of 100 µL. To determine NO-H_2S reactivity, increasing concentration of NO donor sodium nitroprusside (SNP) was added to 10^{-3} M NaHS and allowed to react for 1 min. 50 µM AzMC was then added and incubated for 5 minutes at room temperature. Fluorescence intensity was measured by SpectraMax Gemini EM plate reader (Molecular Devices) at 365 nm excitation and 450 nm emission. Reactivity of AzMC to H_2S was confirmed by adding 50 µM AzMC to increasing NaHS concentrations, as listed.

3.2.6. In vivo coronary vasoreactivity

Coronary tone was evaluated *in vivo* by measuring coronary flow velocity using transthoracic echocardiography as previously described *[67]*. Mice were anesthetized with 1.5% isoflurane and coronary flow velocity was measured using the Vevo 2100 (Visual Sonics) and a 40 MHz transducer (Visual Sonics). The transducer was mounted on a stand (Visual Sonics) to measure flow velocity from the same location for the entire experiment. Chest hair was removed by depilatory cream. The animal was secured onto a heated platform to monitor ECG, heart rate, and body temperature.

Left main coronary artery was visualized by color Doppler flow from a modified long axis view of the left ventricle. Flow velocity profile of the blood flow through the coronary artery was captured by pulse wave velocity. The difference in angle between blood flow and ultrasound beam was accounted for with angle correction done on the Vevo mainframe.

Coronary vasorelaxation was induced by intravenous transfusion of adenosine triphosphate (ATP, Sigma) or beta-adrenergic agonist dobutamine (Dob, Hospira). ATP was administered to evaluate agonist-induced coronary vasorelaxation and dobutamine to evaluate metabolic demand-mediated vasorelaxation. Increase in diameter corresponded with an increase in flow velocity. Drugs were infused through a catheter inserted into the lateral tail vein. Catheters were custom-made by attaching a 30 gauge needle (BD) to size PE-10 polyethylene tubing (BD). Dose of drug administered was controlled with a syringe pump (Harvard Apparatus) by adjusting infusion rate.

Working concentration of ATP was 0.5 mg/mL. ATP was infused at 20, 40, 80, and 160 μg/kg/min for 1 minute per dose. Coronary flow velocity was allowed to return to baseline between each dose. Working concentration of dobutamine was 0.2 mg/mL. Dobutamine was infused at 5, 10, 20, and 30 μg/kg/min at 2 minutes per dose. CSE inhibitor propargylglycine (PPG, Sigma) dissolved in saline was administered intravenously at 50 mg/kg 30 minutes before flow velocity measurements. All drugs were prepared in a heparinized 0.9% saline solution. Peak diastolic flow velocities of three cardiac cycles were measured for data analysis.

3.2.7. Wire myography

Rats were euthanized by isoflurane overdose and left main and descending coronary artery was dissected and sectioned into ~1 mm rings. Precise vessel section length was measured

and vessel sections were mounted onto a wire myograph (DMT). Vessels were bathed in 95/5% O_2/CO_2 oxygenated Krebs physiological solution containing in [mM] 118 NaCl, 4.7 KCl, 25.0 NaHCO3, 1.2 MgSO4, 1.1 KH2PO4, 11 glucose, and 2.5 CaCl2-2H2O maintained at 37°C. Vessels were equilibrated for 30 minutes and then stretched in 0.3 mN increments to the tension equivalent to 50 mmHg (6.7 kPa), as determined by the DMT normalization module for LabChart. After stretching, vessels were equilibrated for 15 minutes, and then subjected to two rounds of 60 mM KCl bolus administration into the bath. Vessels were pre-constricted at 10^{-7} M or $10^{-6.5}$ M U46619 (Cayman) for 15 minutes. Vessels were then subjected to cumulative dose response of NaHS (10^{-5} M, 10^{-4} M, 10^{-3} M; Sigma) or 3-MP (10^{-6} M, 10^{-5} M, 10^{-4} M; Sigma).

To test the involvement of arachadonic acid, rings were next incubated with 10 μM phospholipase A2 inhibitor 4-4(-octadecylphenyl)-4-oxobutenoic acid (OBAA; Tocris) for 30 minutes prior to U46619 pre-constriction, and NaHS and 3-MP dose responses were carried out. Rings were then incubated with 100 μM L-NG-nitroarginine methyl ester (L-NAME; Caymen) to test nitric oxide synthase involvement for 15 minutes prior to U46619 pre-constriction. In a separate experiment, coronary artery rings were mechanically denuded to examine the role of the endothelium in H_2S and 3-MP mediated response.

Acetylcholine (Ach; Sigma) 10^{-5} M was added after NaHS 10^{-3} M and 3-MP 10^{-4} M to determine if endothelial-mediated vasorelaxation function remained intact. In separate challenges, vessels were pre-constricted with U46619 and after steady constriction was reached, 100 μM L-NAME was added. After a steady L-NAME-induced constriction was reached, Ach 10^{-5} M was added to evaluate endothelial-mediated vasorelaxation after NOS inhibition.

3.2.8. Statistical analysis

Statistical significance was determined by two-way analysis of variance with Bonferroni post-test or Student's t-test (GraphPad). Data is reported as mean±SEM.

3.3. RESULTS

3.3.1. CSE and MPST expression in the coronary artery

CSE expression varied between human endothelial cell lines: expression was robust in HAECs and minimal in HCAECs in comparison (Fig. 3.1A). Both cell lines expressed eNOS and MPST in similar abundance.

In rat tissue, CSE was expressed in similar abundance in coronary artery and aorta (Fig. 3.1B). MPST was also expressed in both, although expression was more robust in aortic tissue. Similar abundance of GAPDH confirms equal protein loading between samples.

3.3.2. MPST and CSE-mediated H_2S production in coronary tissue

Enzymatic kinetics of MPST and CSE was characterized in rat liver, where both enzymes are robustly expressed *[68,69]*. Km value of MPST for 3-MP in the reaction conditions was 0.46±0.08 mM 3-MP and Vmax was 254.1±9.6 nM H_2S (Fig. 3.2A). Vmax of CSE for L-cysteine was not reached for the conditions tested so Km of CSE could not be determined (Fig. 3.2B).

To induce maximum enzyme activity, coronary artery homogenate was incubated at twice the Km value for 3-MP and at the highest L-cysteine concentration evaluated. H_2S produced in these conditions were 32.4±6.1 nM for 3-MP incubation and 3.6±6.5 nM for L-cysteine incubation. MPST-mediated production was significantly higher than CSE-mediated production ($p=0.0056$).

3.3.3. Role of CSE-derived H_2S in coronary vasorelaxation in vivo

ATP-mediated vasorelaxation (Fig. 3.3A) was not different between WT, WT treated with PPG, and CSE -/- mice (p=0.33 for WT vs. PPG-treated and p=0.31 for WT vs. CSE -/-). Metabolic demand-mediated vasorelaxation induced by dobutamine (Fig. 3.3B) was also not different between cohorts (p=0.66 for WT vs. PPG-treated and p=0.23 for WT vs. CSE -/-).

3.3.4. Vasoactive effects of exogenous H_2S and 3-MP

3-MP caused dose-dependent vasoconstriction in coronary rings (Fig. 3.4A): 10^{-6} M decreased pre-constriction tone by 3.6±2.2% while 10^{-5} M significantly increased pre-constriction tone by 19.7±9.5% (p=0.022 compared to 3-MP 10^{-6} M), and 10^{-4} M increased pre-constriction tone by 68.6±26%. (p=0.059 compared to 3-MP 10^{-5} M). Vasoconstrictive response to 3-MP was not significantly altered following incubation with PLA2 inhibitor OBAA (p=0.29 OBAA vs. untreated) but was dramatically reduced following NOS inhibition with L-NAME. A dose of 10^{-4} M 3-MP produced an 8.2±4.3% increase in pre-constriction tone with L-NAME incubation compared to 68.6±26.2% increase in tone in untreated vessels (p=0.026). Removal of the endothelium similarly abolished vasoconstrictive effect of 3-MP and unmasked its vasodilatory effect: 10^{-4} M produced a 7.9±6.5% decrease in tone in denuded vessels compared to the 68.6±26.2% increase in tone in endothelial-intact vessels (p=0.034).

NaHS caused dose-dependent vasoconstriction in the coronary arteries (Fig. 3.4B): a 4.9±3.7% increase in pre-constriction tone occurred with 10^{-5} M, 18.3±4.7% increase occurred with 10^{-4} M (p=0.029 vs. 10-5 M), and 218.5±52.0% occurred with 10^{-3} M (p=0.0025 vs. NaHS 10^{-4} M). Following PLA2 inhibition with OBAA, NaHS also produced dose-dependent

vasoconstriction but to a lesser degree: 10^{-5} M produced a 95.9±30.9% increase in pre-constriction tone with OBAA incubation compared to 218.0±52.0% increase in pre-constriction tone in untreated vessels (p=0.039). Following L-NAME incubation, NaHS induced dose-dependent vasodilation: 10^{-5} M NaHS increased pre-constriction tone by 2.8±0.9% while 10^{-4} M NaHS decreased pre-constriction tone by 10.0±7.5% (p=ns compared to NaHS 10^{-5} M). 10^{-3} M NaHS further decreased tone to 76.9±-12.9% of pre-constriction tone (p=0.001 compared to NaHS 10^{-4} M). In endothelial-denuded coronary arteries, NaHS also had little vasoconstrictive effect at 10^{-5} M and 10^{-4} M and induced vasodilation at 10^{-3} M: 10^{-3} M NaHS reduced pre-constriction tone by 76.5±7.9% in denuded vessels compared to 218.5±52.0% increase in tone in endothelial-intact vessels (p=0.00081).

Representative traces of 3-MP dose responses are shown in Fig. 3.5 for untreated (A) and with OBAA incubation (B), L-NAME incubation (C), and endothelial denuding (D) and NaHS dose response for untreated (E), with OBAA incubation (F), L-NAME incubation (G), and endothelial denuding (H).

3.3.5. NO-H_2S interaction

Since enhanced pre-constriction tone could be explained by decreased NO bioavailability, we tested whether H_2S had a direct effect on NOS activity and NO production. Maximum endothelial-mediated vasorelaxation with 10^{-5} M Ach was not different between vessels pre-constricted only with U46619 and vessels that exhibited increased pre-constriction tension from the addition of 10^{-3} M NaHS or 10^{-4} M 3-MP (Fig. 3.6A). Ach-induced vasorelaxation was 86.0±2.4% for U46619 only pre-constricted vessels compared to 81.0±7.2% relaxation for vessels with enhanced pre-constriction tone from NaHS and 72.7±8.6% relaxation

for vessels with increased pre-constriction tone from 3-MP. Ach-induced vasorelaxation was also not significantly reduced with L-NAME incubation compared to untreated vessels: vasorelaxation was 65.5±21.4% with L-NAME incubation compared to 86.0±2.4% in untreated U46619 only vessels.

We next tested whether NO could directly interact with H_2S. Fluorescence intensity increased with increasing dose of NaHS, demonstrating that AzMC reacted with NaHS (Fig. 3.6B). Increasing SNP concentration caused decreasing fluorescence intensity and therefore H_2S availability (Fig. 3.6C).

3.4. DISCUSSION

We investigated the role of H_2S and the contribution of vascular H_2S producers CSE and MPST in coronary tone vasoregulation. We demonstrate that CSE is not a significant contributor to coronary vasoregulation and provide evidence that supports the involvement of MPST in coronary vasoregulation. We further describe H_2S as a coronary vasoconstrictor when NO bioavailability is physiological and vasodilator in the absence of NO.

Protein abundance measurement by Western blot showed that CSE and MPST are expressed in human and rat vascular tissue, although the relative expression between vascular beds varies between the two species. CSE expression in HCAECs was slight compared to HAECs and MPST expression was similar between the cell lines. In contrast, CSE expression was similar between rat coronary and rat aorta while MPST expression was robust in the aorta and slight in the coronary artery. The difference in expression could be due to species differences. Alternatively, the inconsistency could be due to differences in vascular health. CSE and MPST expression have been shown to be influenced by pathological conditions. In a mouse

heart failure model, mice with heart failure induced by thoracic aortic constriction had elevated CSE expression and reduced MPST expression in the cardiac tissue *[70]*. While the rats from which the tissue was harvested can be considered healthy, we did not ascertain the vascular health status of the donors of the human cell lines. Nevertheless, both sets of protein expression data demonstrate that both CSE and MPST are expressed in the coronary artery and support the possibility of endogenous H_2S production in the coronary vasculature.

Michaelis-Menten kinetics of CSE and MPST were examined *in vitro* using rat liver homogenate. For 3-MP, the Km value was 0.46±0.14 mM 3-MP. The CSE reaction did not reach Vmax at 50 mM L-cysteine, a concentration far exceeding physiologically relevant L-cysteine values. Previously reported Km values is 1.2±0.1 mM 3-MP for wild-type rat liver-derived MPST *[68]* and 1.9 mM L-cysteine for wild-type human CSE *[71]*. Differences in reported values can be attributed to reaction conditions. In the previous studies, both reactions were performed at basic pH, pH 9.55 for the MPST reaction and pH 8.2 for the CSE reaction, while the reactions in this study were performed at pH 7.0. The Km value of human CSE for L-cysteine has also been shown to vary significantly with polymorphic variants *[72]*.

In vitro amperometric H_2S measurement showed that H_2S produced through the MPST pathway was significantly greater than through the CSE pathway. Enzymatic activity conditions, however, were not equivalent. The MPST reaction was performed at twice the Km value of MPST, thereby maximizing MPST activity. The CSE reaction was performed at the highest substrate concentration tested in the liver homogenate, 50 mM. While this L-cysteine concentration is presumably less than the Km of the enzyme, it is significantly higher than concentrations that are physiologically relevant. Even under supra-physiological substrate concentrations, amperometric signal did not increase significantly above baseline, supporting

that under physiological conditions, H_2S production does not appear to be mediated by CSE. In comparison, a significant increase in amperometric signal from baseline with 3-MP incubation supports that MPST is a source of endogenous H_2S in the coronary vasculature.

In vivo coronary vasorelaxation response in CSE-deficient and CSE-inhibited mice were not different from untreated wild-type mice. In conjunction with the lack of CSE-mediated H_2S production *in vitro*, these *in vivo* data further support the notion that CSE-derived H_2S does not significantly contribute to coronary vasoregulation. Our findings are confirmed by previous studies that reported lack of coronary vasodilation upon addition of L-cysteine, suggesting minimal involvement of CSE in coronary tone modulation *[61,64]*. The insignificant role of CSE-produced H_2S in the coronary vasculature seems counterintuitive given the significant role of CSE-produced H_2S in regulating tone of the resistance arteries *[57]*. However, endothelial protein expression and associated phenotypic traits have been shown to vary by vascular bed. For instance, in the heart, endocardial endothelial cells express connexin (CX) 43, CX40, and CX37 while myocardial capillary endothelial cells do not, consistent with the observation that endocardial endothelial cells possess a larger number of gap junctions than myocardial endothelial cells *[73]*. It is therefore not an unreasonable possibility that the coronary arteries, which are controlled locally, have different main vasoactive mediators than the resistance arteries, which are controlled neurohumorally.

We demonstrated *in vitro* that the coronary artery can produce H_2S by the MPST pathway. Because direct MPST inhibitors are currently unavailable and transgenic deletion model was not readily accessible, we determined if MPST was important physiologically using *ex vivo* wire myography. Vasoactive response to MPST substrate 3-MP was similar to the vasoactive response to H_2S donor NaHS. The vasoconstrictive effects were not significantly

altered with PLA2 inhibition but disappeared with NOS inhibition and endothelial denudation. These data support that the effects of 3-MP are mediated through MPST production of H_2S as opposed to direct vascular effects of 3-MP. Although 3-MP-induced vasoconstriction was removed by L-NAME incubation and endothelial removal, 3-MP was not observed to induce vasodilation to the same degree as NaHS. Lack of vasodilatory effects of 3-MP could be due to insufficient substrate amount to produce the amount of H_2S necessary for vasodilation. Coronary vasodilation was observed in this study, and has been previously reported, to occur at 1 mM NaHS. This concentration of H_2S may not have been possible to produce *in vivo* with the 3-MP concentration used.

Interestingly, we observe vasoconstrictive effects of NaHS in untreated coronary arteries, which contradicts previous studies that reported vasodilatory effects of NaHS *[61-64]*. However, NaHS dose response conducted simultaneously in aortic rings from the same experimental animals (Fig. 3.7) was consistent with published findings of the dual effect of NaHS in rat aorta *[60,74]*. The vasoconstrictive effect of NaHS in the coronary artery described in this study is therefore not an artifact of differences in experimental procedure. We demonstrate, however, that the vasoconstrictive effect of NaHS is eNOS and therefore NO dependent. NOS inhibition with L-NAME yielded no vasoconstriction and only vasodilation. Similar response observed with endothelial denuding identified the involvement of eNOS and eNOS-derived NO.

Reducing NO bioavailability through eNOS inhibition has been shown to further increase pre-constriction tension *[42]*. The enhanced vasoconstriction with addition of NaHS observed in this study could therefore occur through eNOS inhibition or NO scavenging. Both H_2S interference with eNOS activity as well as H_2S reaction with NO have been previously

described. H_2S was shown to cause a dose-dependent decrease in activity of recombinant bovine eNOS. The resulting reduction in NO bioavailability was associated with the observed vasoconstrictive effects of NaHS in rat and mouse aorta *[60]*. Aortic vasoconstriction observed at low NaHS doses was attributed to the vasoconstrictive effects of reduced NO bioavailability overriding the vasodilatory effects of H_2S. Aortic vasodilation observed at high NaHS doses was attributed to the vasodilatory effects of H_2S overriding the vasoconstrictive effects of decreased NO bioavailability. The reported H_2S inhibition of eNOS appears to contradict other studies that demonstrated that exogenous H_2S promoted eNOS function and eNOS production of NO *[74,75]*. However, the duration of the exogenous H_2S administration was different between the studies. H_2S donor treatment was chronic in the studies showing cooperative effects of H_2S on eNOS function and acute in the study that showed dose-dependent decrease in eNOS activity as well as this study. H_2S has also been shown to react with NO to form a nitrosothiol, demonstrating the scavenging effect of H_2S. Mixing NaHS with SNP reduced the vasodilatory effects of SNP in pre-constricted rat aortic rings, further supporting that H_2S reacted with NO and reduced NO bioavailability through scavenging *[74,76]*.

Our *ex vivo* vasoreactivity data showed that endothelial-mediated relaxation was maximal after NaHS-induced vasoconstriction. NOS inhibition with L-NAME also did not significantly attenuate endothelial-mediated relaxation, which would suggest that eNOS activity cannot be evaluated by maximum Ach-induced relaxation. However, we note that the addition of 10^{-5} M Ach after L-NAME incubation resulted in complete relaxation in some ring sections and no vasorelaxation in other sections from the same animal. This dual effect when averaged resulted in overall minimal impairment of Ach-induced vasorelaxation with a large standard error. 10^{-5} M Ach consistently induced complete relaxation between ring sections and animals for both

NaHS and 3-MP, supporting that eNOS activity was truly unimpaired. This *ex vivo* vasoreactivity data therefore support that H_2S-induced vasoconstriction is not through inhibition of eNOS activity.

Our fluorometric data demonstrated the scavenging interaction of H_2S and NO. Whether the reaction product of H_2S and NO is also a vasoconstrictor was not tested in this study. However, as noted earlier, this reaction product was shown previously to not have vasoactive effects *[74,76]*.

Vasoconstriction observed in this study can therefore be attributed directly to decreased NO bioavailability. Because only the vasodilatory effects of NaHS were observed in the absence of NO, either by L-NAME inhibition or by endothelial denuding, we agree that H_2S is a vasodilator in the coronary vasculature. We further conclude that its vasoconstrictive effects are due to its scavenging interaction with NO. The NO-dependency of the vasoactive effects of H_2S suggests a change in role from regulatory to vasodilatory with development of coronary artery disease. Under healthy conditions with physiological NO bioavailability, H_2S appears to primarily regulate NO. In disease conditions with diminished NO bioavailability, H_2S could serve as a compensatory vasomediator. By extension, these findings support that exogenous H_2S induces vasoconstriction in healthy coronary arteries and vasodilation in diseased coronary arteries. Therapies involving administration of exogenous H_2S would therefore benefit coronary artery disease patients but would be counterproductive as a supplement for patients with healthy coronary arteries.

A limitation of this is study is the absence of H_2S measurement in the bath during the wire myograph experiments to confirm that the effects of 3-MP are due to MPST-mediated H_2S production. This detection was limited by the sensitivity of the amperometric probe in a noisy

environment. Nevertheless, similar effects and mechanism of action between 3-MP and NaHS support the conclusion that 3-MP is acting on the coronary artery through H_2S production by MPST.

3.5. FIGURES

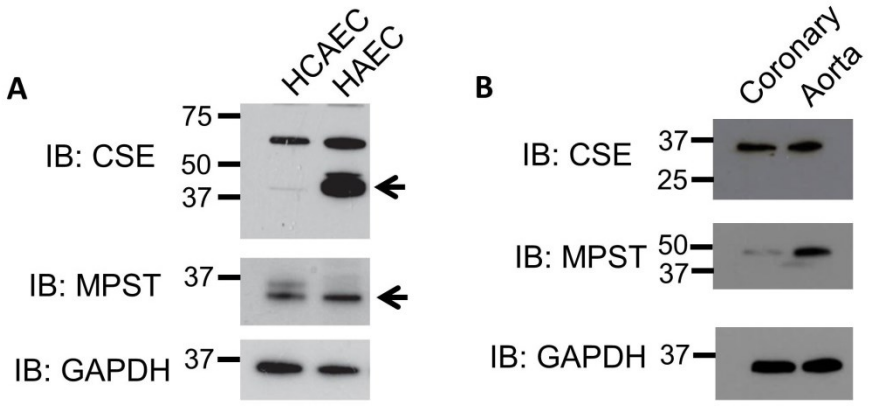

Figure 3.1. CSE and MPST expression in the coronary artery. Protein expression was measured in coronary endothelial cells from human (HCAECs) (A) and intact coronary artery from rat (B). Human aortic endothelial cells (HAECs) and rat aorta were used as positive controls. CSE expression in HCAECs was not as robust as in HAECs. MPST expression was similar between the two cell lines. Rat coronary expressed CSE in similar abundance as rat aorta. However, MPST expression was lower in rat coronary compared to rat aorta. GAPDH was use as loading control.

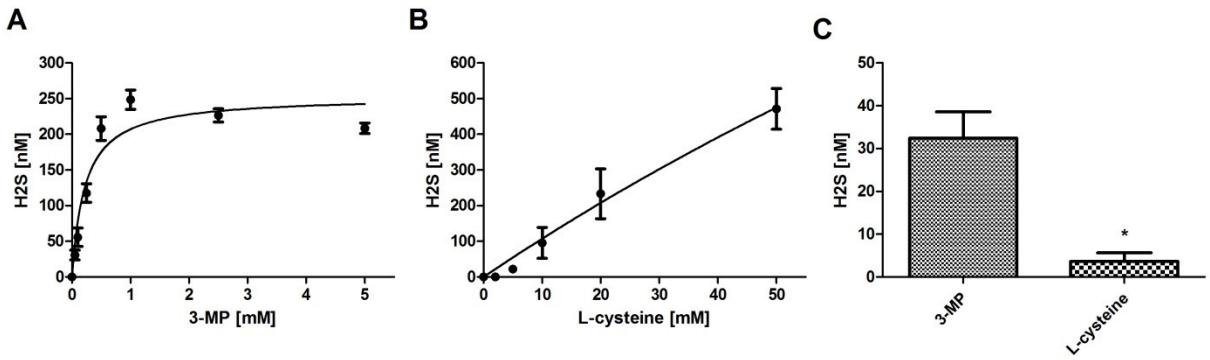

Figure 3.2. *In vitro* amperometric measurement of tissue H_2S production. Michaelis-Menten kinetics of MPST was characterized in rat liver homogenate by measuring amount of H_2S produced by increasing concentrations of 3-MP (A). Km of MPST was 0.46±0.14 mM. Kinetic behavior of CSE was evaluated by measuring amount of H_2S produced by increasing concentration of L-cysteine (B). Km and Vmax of CSE was not reached under the conditions tested. For coronary H_2S production, rat coronary homogenate was incubated in 1mM 3-MP to measure MPST-mediated H_2S production and in 50mM L-cysteine to measure CSE-mediated H_2S production (C). Amperometric signal was significantly greater with 3-MP incubation than L-cysteine incubation, *$p<0.05$.

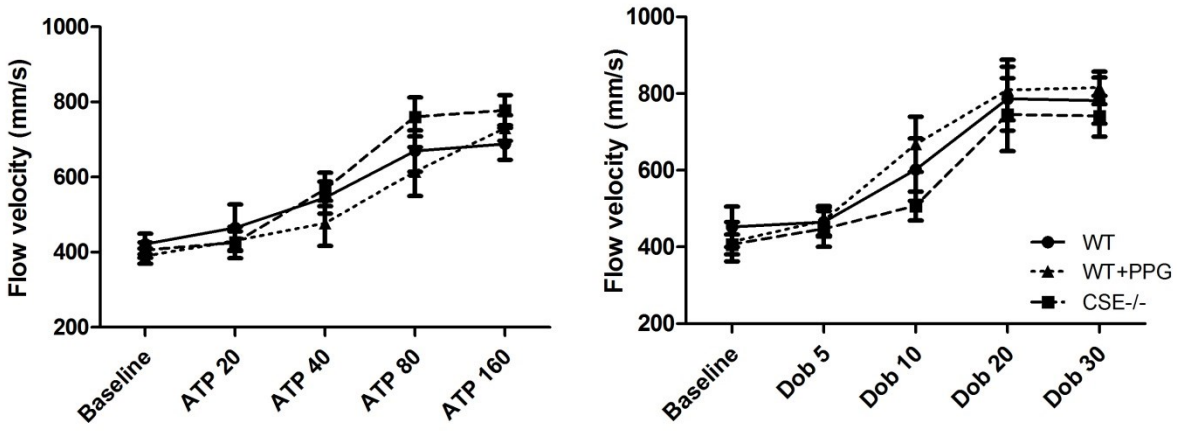

Figure 3.3. *In vivo* coronary vasorelaxation in CSE knockout and pharmacologically-inhibited mice. Coronary vasorelaxation function was evaluated *in vivo* by measuring increase in flow velocity using high-resolution ultrasound. Dose-dependent increase in flow velocity to ATP, representing agonst-induced vasorelaxation, and dobutamine, representing metabolic demand-induced vasorelaxation, were obtained. CSE activity was inhibited by intravenous administration of 50 mg/kg propargylglycine (PPG) 30 minutes before flow velocity measurement. ATP-induced vasorelaxation response was not different between wild-type (WT), PPG-treated wild-type, and CSE knockout mice (A). Vasorelaxation response to dobutamine-induced increase in cardiac metabolic demand was also not different between cohorts (B).

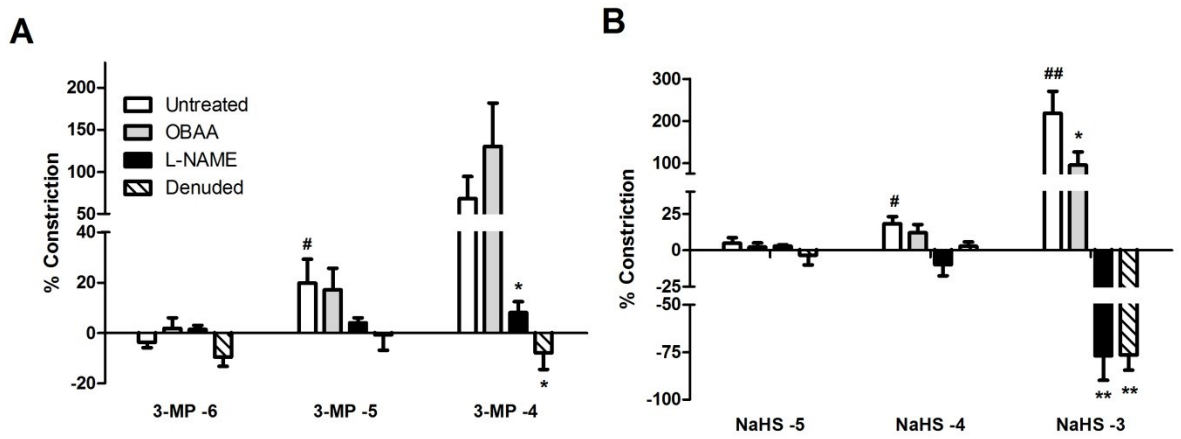

Figure 3.4. Vasoactive effects of 3-MP and NaHS. Physiological role of MPST in coronary vasoregulation was determined by wire myography in the rat left coronary artery. Data is displayed as percent change from pre-constriction tone. 3-MP induced vasoconstriction in pre-constricted arteries in a dose-dependent manner (A). Incubation with 10 μM phospholipase 2A inhibitor OBAA did not alter 3-MP vasoconstrictive effects. 100 μM L-NAME incubation significantly reduced 3-MP-mediated vasoconstriction. Endothelial removal resulted in 3-MP mediated vasodilation. Exogenous H_2S donor NaHS also induced vasoconstriction in pre-constricted arteries in a dose-dependent manner (B). OBAA incubation attenuated NaHS-induced vasoconstriction. L-NAME and endothelial denuding removed NaHS-induced vasoconstriction and only presented NaHS-induced vasodilation. # $p<0.05$ and ## $p<0.01$ comparing between previous dose within the same treatment group; * $p<0.05$ and ** $p<0.01$ when comparing treated groups with untreated within a dose.

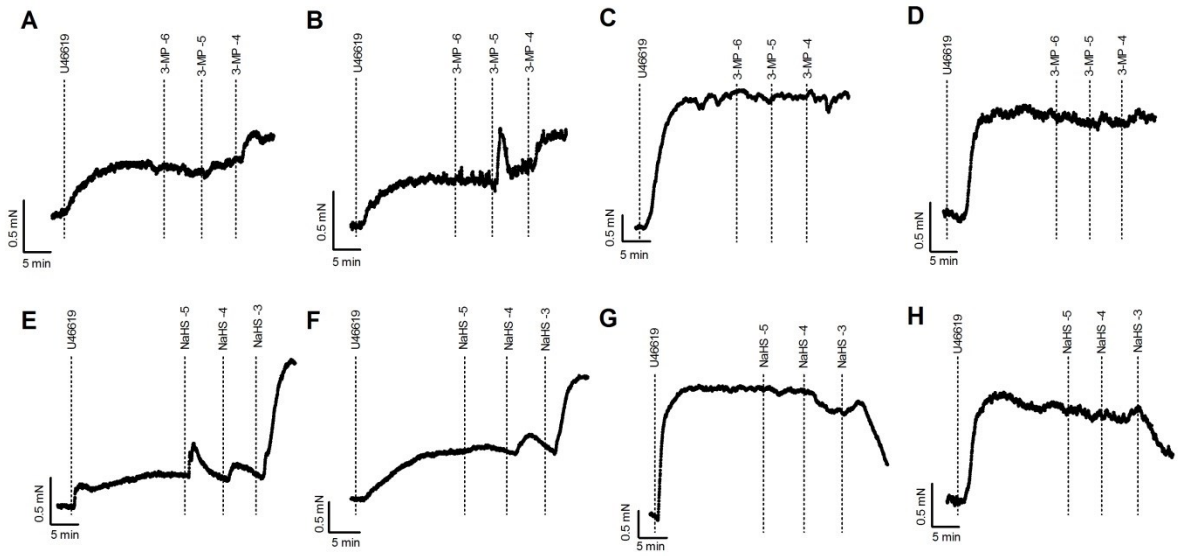

Figure 3.5. 3-MP and NaHS dose response traces. Representative vasotension traces of 3-MP dose response in untreated coronary artery (A) and after incubation with 10 μM OBAA (B) and 100 μM L-NAME (C) and endothelial denudation (D). NaHS dose response in untreated coronary artery (E), after OBAA incubation (F), L-NAME (G), and endothelial denudation (H).

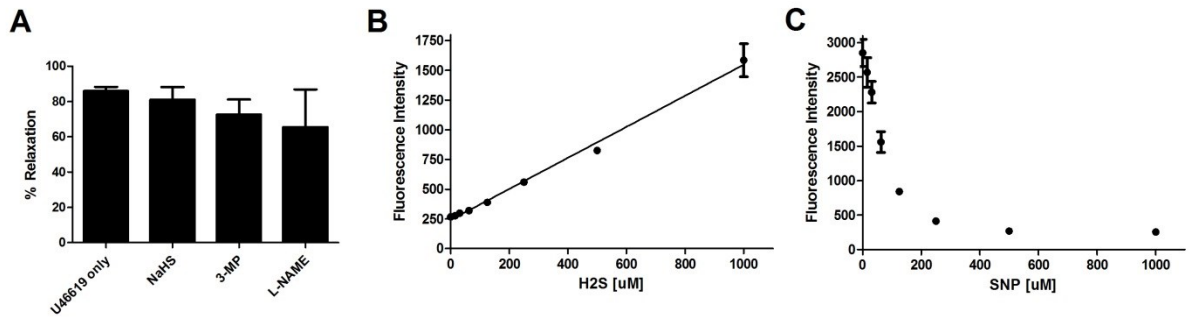

Figure 3.6. H_2S-mediated vasoconstriction via reduced eNOS activity and decreased NO bioavailability. eNOS activity was measured by percent relaxation with addition of 10^{-5} M acetylcholine (Ach) bolus after maximum increase in pre-constriction tension induced by NaHS, 3-MP, or L-NAME (A). Ach relaxation response was compared to vessels pre-constricted with U46619 only. Maximum Ach-induced endothelial-mediated relaxation was not different between U46619 only and NaHS, 3-MP, and L-NAME-constricted vessels. H_2S effect on NO bioavailability was measured *in vitro* by fluorometric probe 7-azido methylcoumarin (AzMC). Fluorescence intensity of AzCM increased with H_2S dose (B). Addition of increasing dose of NO donor sodium nitroprusside (SNP) to 10^{-3} M NaHS resulted in a dose-dependent decrease in fluorescence intensity (C).

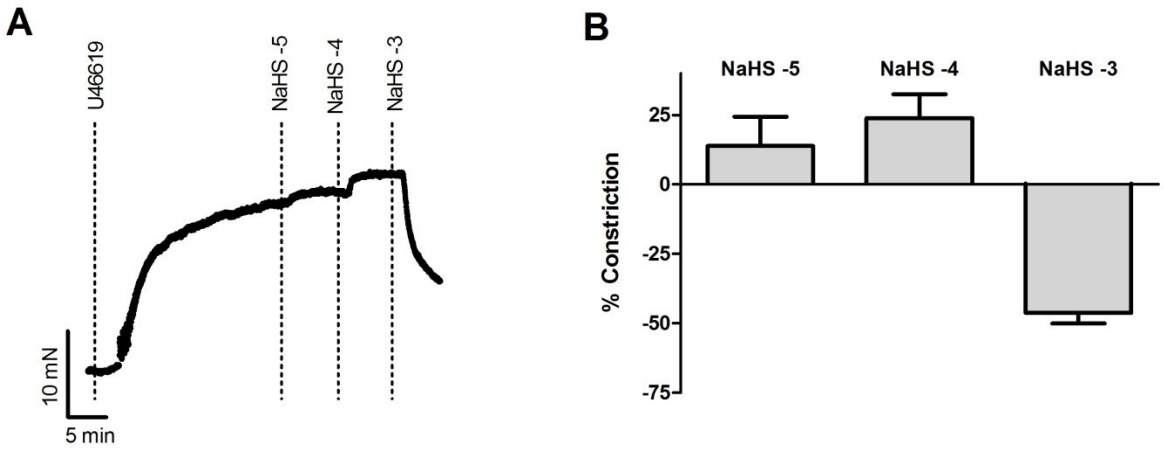

Figure 3.7. Vasoactive effects of NaHS in rat aorta. Representative trace of NaHS dose response (A). NaHS causes vasoconstriction at lower doses and vasodilation at higher doses (B), consistent with previously published findings.

SUMMARY & FUTURE DIRECTIONS

Chapter 2 examined whether ionizing radiation exposure initiated the same mechanistic events that promote the development of coronary artery disease, namely increased superoxide production occurring with impaired coronary endothelial function. Rats exposed to ionizing radiation exhibited reduced coronary flow *in vivo*. Decreased coronary flow was associated with both decreased aortic diastolic pressure and elevated superoxide content in the coronary artery. Diminished diastolic pressure was attributed to decreased heart rate. Reduction of superoxide production by xanthine oxidase inhibition partially restored basal coronary flow and coronary superoxide content. However, *in vivo* vasodilatory response was not improved. Moreover, endothelial function was preserved in irradiated rats. These findings support that radiation-associated coronary artery disease is initiated by increased superoxide level, which leads to reduced NO bioavailability and diminished coronary vasodilatory response *in vivo*. The data further suggest that excess superoxide production precedes coronary endothelial dysfunction characteristic of coronary artery disease.

These findings support that targeting excess ROS production can potentially prevent future development of coronary artery disease. Pre-emptive activation of the nuclear factor-like 2 (Nrf2)-controlled antioxidant response pathway is a promising intervention method. Several studies have demonstrated the benefits of Nrf2 activation in protecting cells from oxidative damage. Radioresistance of cancer cells was attributed to constitutively active Nrf2 pathway *[77]* while compounds that enhanced cell survival after radiation exposure were shown to work through Nrf2 *[78,79]*. Moreover, a number of food sources can activate Nrf2, including sulforaphane found in broccoli sprouts and resveratrol found in red wine. Nrf2-based

interventions are therefore potentially easy to implement for defense against occupation-associated ionizing radiation exposure.

Chapter 3 investigated the role of endogenously produced H_2S in regulating coronary tone. Both vascular H_2S producing enzymes cystathionine gamma lyase (CSE) and mercaptopyruvate sulfertransferase (MPST) proteins were detected in human coronary endothelial cells and rat coronary arteries. *In vitro* measurement of H_2S production showed that the rat coronary artery can produce H_2S through the MPST pathway but not through the CSE pathway. Both pharmacologic inhibition and genetic deletion of CSE did not alter coronary vasodilatory function *in vivo,* supporting that CSE-produced H_2S does not have a significant role in coronary vasoregulation. *Ex vivo* coronary vasoreactivity response to MPST substrate 3-mercaptopyruvate (3-MP) was similar to the vasoreactivity response to H_2S donor sodium hydrosulfide (NaHS), supporting that vasoactive effects of 3-MP were through MPST-mediated production of H_2S. The data demonstrate that H_2S production in the coronary artery is mediated by MPST and not CSE, contrary to other vascular beds where CSE has a significant role. The data further show that the vasoactive effect of H_2S is NO dependent: H_2S induces coronary vasoconstriction in the presence of NO and vasorelaxation in the absence of NO. Vasoconstrictive effects of H_2S appear to be due to its scavenging of NO and the resulting decrease in NO bioavailability.

These findings are particularly intriguing when considering the potential contraindications of H_2S-based treatments for heart disease. H_2S is associated with promoting cardiovascular health. Besides gaseous H_2S, H_2S can be supplied from dietary sources, notably garlic. In fact, the cardiovascular benefits of garlic were shown to be a result of its H_2S donor properties *[80]*. Dietary H_2S supplementation therefore could promote coronary vasodilation

and cardiac health in coronary artery disease patients. In healthy patients, however, or patients with less severe coronary artery disease, exogenous supplementation may have adverse effects because the vasoconstrictive properties of H_2S would be more relevant.

Another interesting application is sulfhydryl-containing angiotensin converting enzyme (ACE) inhibitors. Sulfhydryl-ACE inhibitor zofenopril has been reported to have additional beneficial effects compared to dicarobxylate-ACE inhibitors, including improved clinical outcomes in patients with acute myocardial infarction and congestive failure as well as improved flow-mediated vasodilation. The beneficial effects of zofenopril recently were shown to be due to its H_2S donor properties *[81]*. As ACE inhibitors are administered to heart disease patients who would most likely have diminished NO bioavailability, the vasoconstrictive effects of H_2S released by zofenopril may not be problematic. However, for patients with less severe symptoms, the vasoconstrictive effects may manifest. Further examination of the vasoactive influences of exogenous H_2S donors on the coronary artery would clarify potential adverse effects of these treatments.

CONCLUDING REMARKS

This dissertation demonstrates the use of novel ultrasound-based methods to evaluate coronary and vascular function. Moreover, this dissertation illustrates how altering the bioavailability of NO influences coronary vasodilatory function as well as the roles of other vasoactive mediators in coronary vasoregulation. Chapter 2 demonstrated how reduced coronary vasoreactivity *in vivo* did not arise from impaired endothelial or smooth muscle function, but excess scavenging of NO by elevated coronary ROS content. Chapter 3 showed how the role of MPST-produced H_2S changed with NO bioavailability: H_2S induced vasoconstriction in the presence of NO and vasodilation in the absence of NO.

These studies could suggest H_2S as a vanguard compensatory molecule in the absence of NO. However, in a situation of decreased NO bioavailability, H_2S may still act as a regulatory molecule. This role would explain why after ionizing radiation exposure, where the increased ROS presumably decreases NO bioavailability, basal coronary flow is not preserved. H_2S also may not be a potent compensatory mechanism as the vasodilatory effects of H_2S are observed only at higher concentrations. Moreover, most pathological vascular conditions are associated with reduced NO bioavailability and not complete absence of NO. Nevertheless, these studies reinforce the importance of NO in regulating coronary tone.

This dissertation also demonstrates how changes in *in vivo* response may not be reflected in the *ex vivo* measurement. In Chapter 2, attenuated vasodilatory response observed *in vivo* did not correspond to impaired *ex vivo* vasodilatory response. In Chapter 3, increased aortic stiffness observed *in vivo* was not associated with increased stiffness measured *ex vivo*. These findings show the significance of *in vivo* influences on vascular function and further illustrate the power of implementing a multi-level approach in studying vascular function. Changes in cellular

signaling can be correlated to changes in physiological function, providing a more complete representation of vascular function after the introduction of a pathogenic stimulus.

REFERENCES

1. Nakanishi K, Fukuda S, Shimada K, Miyazaki C, Otsuka K, Maeda K, et al. Impaired coronary flow reserve as a marker of microvascular dysfunction to predict long-term cardiovascular outcomes, acute coronary syndrome and the development of heart failure. Circ J 2012; 76:1958-64.
2. Wikstrom J, Gronros J, Bergstrom G, Gan LM. Functional and morphologic imaging of coronary atherosclerosis in living mice using high-resolution color doppler echocardiography and ultrasound biomicroscopy. J Am Coll Cardiol 2005; 46:720-27.
3. White TD, Angus JA. Relaxant effects of atp and adenosine on canine large and small coronary-arteries invitro. European Journal of Pharmacology 1987; 143:119-26.
4. Gordon JL. Extracellular atp - effects, sources and fate. Biochem J 1986; 233:309-19.
5. Gorman MW, Ogimoto K, Savage MV, Jacobson KA, Feigl EO. Nucleotide coronary vasodilation in guinea pig hearts. American Journal of Physiology - Heart and Circulatory Physiology 2003; 285:H1040-H47.
6. Bender SB, Berwick ZC, Laughlin MH, Tune JD. Functional contribution of p2y1 receptors to the control fo coronary blood flow. J Appl Physiol 2011; 111:1744-50.
7. Mitchell GF, Parise H, Benjamin EJ, Larson MG, Keyes MJ, Vita JA, et al. Changes in arterial stiffness and wave reflection with advancing age in healthy men and women - the framingham heart study. Hypertension 2004; 43:1239-45.
8. Mahmud A, Feely J. Effect of smoking on arterial stiffness and pulse pressure amplification. Hypertension 2003; 41:183-7.
9. Lehmann ED, Gosling RG, Sonksen PH. Arterial wall compliance in diabetes. Diabet Med 1992; 9:114-9.
10. Wang Y-X, Fitch R, Li W, Werner M, Halks-Miller M, Lillis B, et al. Reduction of cardiac functional reserve and elevation of aortic stiffness in hyperlipidemic yucatan minipigs with systemic and coronary atherosclerosis. Vasc Pharmacol 2002; 39:69-76.
11. Ben-Shlomo Y, Spears M, Boustred C, May M, Anderson SG, Benjamin EJ, et al. Aortic pulse wave velocity improves cardiovascular event prediction: An individual participant meta-analysis of prospective observational data from 17,635 subjects. J Am Coll Cardiol 2014; 63:636-46.
12. Mitchell GF, Hwang SJ, Vasan RS, Larson MG, Pencina MJ, Hamburg NM, et al. Arterial stiffness and cardiovascular events: The framingham heart study. Circulation 2010; 121:505-11.
13. Mattace-Raso FU, van der Cammen TJ, Hofman A, van Popele NM, Bos ML, Schalekamp MA, et al. Arterial stiffness and risk of coronary heart disease and stroke: The rotterdam study. Circulation 2006; 113:657-63.
14. Laurent S, Boutouyrie P, Asmar R, Gautier I, Laloux B, Guize L, et al. Aortic stiffness is an independent predictor of all-cause and cardiovascular mortality in hypertensive patients. Hypertension 2001; 37:1236-41.
15. Fung YC. *Biomechanics: Mechanical properties of living tissues.* 2nd ed. New York, NY: Springer; 1993.
16. Shadwick RE. Mechanical design in arteries. J Exp Biol 1999; 202:3305-13.
17. Gasser TC, Ogden RW, Holzapfel GA. Hyperelastic modelling of arterial layers with distributed collagen fibre orientations. Journal of The Royal Society Interface 2006; 3:15-35.
18. Zieman SJ, Melenovsky V, Kass DA. Mechanisms, pathophysiology, and therapy of arterial stiffness. Arteriosclerosis, Thrombosis, and Vascular Biology 2005; 25:932-43.
19. Jung SM, Jandu S, Steppan J, Belkin A, An SS, Pak A, et al. Increased tissue transglutaminase activity contributes to central vascular stiffness in enos knockout mice. Am J Physiol-Heart Circul Physiol 2013; 305:H803-H10.

20. Santhanam L, Tuday EC, Webb AK, Dowzicky P, Kim JH, Oh YJ, et al. Decreased s-nitrosylation of tissue transglutaminase contributes to age-related increases in vascular stiffness. CircRes 2010; 107:117-U243.
21. Fitch RM, Vergona R, Sullivan ME, Wang YX. Nitric oxide synthase inhibition increases aortic stiffness measured by pulse wave velocity in rats. Cardiovasc Res 2001; 51:351-58.
22. Bergel DH. The static elastic properties of the arterial wall. The Journal of Physiology 1961; 156:445-57.
23. Leloup AJ, Fransen P, Van Hove CE, Demolder M, De Keulenaer GW, Schrijvers DM. Applanation tonometry in mice: A novel noninvasive technique to assess pulse wave velocity and arterial stiffness. Hypertension 2014; 21:21.
24. Morrison TM, Choi G, Zarins CK, Taylor CA. Circumferential and longitudinal cyclic strain of the human thoracic aorta: Age-related changes. J Vasc Surg 2009; 49:1029-36.
25. Butlin M, Hammond A, Lindesay G, Viegas K, Avolio AP. 138 in-vitro and in vivo use of vasoactive agents in characterising aortic stiffness in rats: Testing the assumptions. J Hypertens 2012; 30:e42 10.1097/01.hjh.0000419960.98375.d3.
26. Kuo MM, Barodka V, Abraham TP, Steppan J, Shoukas AA, Butlin M, et al. Measuring ascending aortic stiffness *in vivo* in mice using ultrasound. J Vis Exp 2014; e52200.
27. Darby SC, Ewertz M, McGale P, Bennet AM, Blom-Goldman U, Bronnum D, et al. Risk of ischemic heart disease in women after radiotherapy for breast cancer. N Engl J Med 2013; 368:987-98.
28. Boivin JF, Hutchison GB, Lubin JH, Mauch P. Coronary artery disease mortality in patients treated for hodgkin's disease. Cancer 1992; 69:1241-7.
29. Shimizu Y, Kodama K, Nishi N, Kasagi F, Suyama A, Soda M, et al. Radiation exposure and circulatory disease risk: Hiroshima and nagasaki atomic bomb survivor data, 1950-2003. Bmj 2010; 14.
30. Kannel WB, Gordon T, Schwartz MJ. Systolic versus diastolic blood pressure and risk of coronary heart disease: The framingham study. The American Journal of Cardiology 1971; 27:335-46.
31. Kinlay S, Libby P, Ganz P. Endothelial function and coronary artery disease. Curr Opin Lipidology 2001; 12:383-89.
32. Schachinger V, Britten MB, Zeiher AM. Prognostic impact of coronary vasodilator dysfunction on adverse long-term outcome of coronary heart disease. Circulation 2000; 101:1899-906.
33. van Leeuwen-Segarceanu EM, Dorresteijn LDA, Vogels OJM, Biesma DH, Bos WJW. Arterial stiffness is increased in hodgkin lymphoma survivors treated with radiotherapy. Leuk Lymphoma 2013; 54:1734-41.
34. Sasaki H, Wong FL, Yamada M, Kodama K. The effects of aging and radiation exposure on blood pressure levels of atomic bomb survivors. Journal of Clinical Epidemiology 2002; 55:974-81.
35. Beckman JA, Thakore A, Kalinowski BH, Harris JR, Creager MA. Radiation therapy impairs endothelium-dependent vasodilation in humans. J Am Coll Cardiol 2001; 37:761-65.
36. Stamler JS, Singel DJ, Loscalzo J. Biochemistry of nitric oxide and its redox-activated forms. Science 1992; 258:1898-902.
37. Dhalla NS, Temsah RM, Netticadan T. Role of oxidative stress in cardiovascular diseases. J Hypertens 2000; 18:655-73.
38. Spiekermann S, Landmesser U, Dikalov S, Bredt M, Gamez G, Tatge H, et al. Electron spin resonance characterization of vascular xanthine and nad(p)h oxidase activity in patients with coronary artery disease - relation to endothelium-dependent vasodilation. Circulation 2003; 107:1383-89.
39. Soucy KG, Lim HK, Benjo A, Santhanam L, Ryoo S, Shoukas AA, et al. Single exposure gamma-irradiation amplifies xanthine oxidase activity and induces endothelial dysfunction in rat aorta. Radiat Environ Biophys 2007; 46:179-86.

40. Soucy KG, Lim HK, Attarzadeh DO, Santhanam L, Kim JH, Bhunia AK, et al. Dietary inhibition of xanthine oxidase attenuates radiation-induced endothelial dysfunction in rat aorta. J Appl Physiol 2010; 108:1250-58.
41. Baldus S, Koster R, Chumley P, Heitzer T, Rudolph V, Ostad MA, et al. Oxypurinol improves coronary and peripheral endothelial function in patients with coronary artery disease. Free Radic Biol Med 2005; 39:1184-90.
42. Moore PK, Alswayeh OA, Chong NWS, Evans RA, Gibson A. L-ng-nitro arginine (l-noarg), a novel, l-arginine-reversible inhibitor of endothelium-dependent vasodilatation invitro. Br J Pharmacol 1990; 99:408-12.
43. Chu A, Chambers DE, Lin CC, Kuehl WD, Cobb FR. Nitric oxide modulates epicardial coronary basal vasomotor tone in awake dogs. Am J Physiol 1990; 258:H1250-4.
44. Kelm M, Schrader J. Control of coronary vascular tone by nitric oxide. Circ Res 1990; 66:1561-75.
45. Veinot JP, Edwards WD. Pathology of radiation-induced heart disease: A surgical and autopsy study of 27 cases. Hum Pathol 1996; 27:766-73.
46. van der Loo B, Labugger R, Skepper JN, Bachschmid M, Kilo J, Powell JM, et al. Enhanced peroxynitrite formation is associated with vascular aging. The Journal of Experimental Medicine 2000; 192:1731-44.
47. White M, Roden R, Minobe W, Khan MF, Larrabee P, Wollmering M, et al. Age-related changes in beta-adrenergic neuroeffector systems in the human heart. Circulation 1994; 90:1225-38.
48. Timmermans R, Gerber GB. The effect of x irradiation on cardiac β-adrenergic receptors in the rabbit. Radiat Res 1984; 100:510-18.
49. Jones LF, Brody MJ. Coronary blood-flow in rats is dependent on the release of vascular nitric-oxide. J Pharmacol Exp Ther 1992; 260:627-31.
50. Shiode N, Morishima N, Nakayama K, Yamagata T, Matsuura H, Kajiyama G. Flow-mediated vasodilation of human epicardial coronary arteries: Effect of inhibition of nitric oxide synthesis. J Am Coll Cardiol 1996; 27:304-10.
51. Quyyumi AA, Dakak N, Andrews NP, Gilligan DM, Panza JA, Cannon RO. Contribution of nitric-oxide to metabolic coronary vasodilation in the human heart. Circulation 1995; 92:320-26.
52. Yada T, Shimokawa H, Hiramatsu O, Kajita T, Shigeto F, Goto M, et al. Hydrogen peroxide, an endogenous endothelium-derived hyperpolarizing factor, plays an important role in coronary autoregulation in vivo. Circulation 2003; 107:1040-45.
53. Yada T, Shimokawa H, Hiramatsu O, Shinozaki Y, Mori H, Goto M, et al. Important role of endogenous hydrogen peroxide in pacing-induced metabolic coronary vasodilation in dogs in vivo. J Am Coll Cardiol 2007; 50:1272-78.
54. Canty JM, Schwartz JS. Nitric-oxide mediates flow-dependent epicardial coronary vasodilation to changes in pulse frequency but not mean flow in conscious dogs. Circulation 1994; 89:375-84.
55. Shibuya N, Mikami Y, Kimura Y, Nagahara N, Kimura H. Vascular endothelium expresses 3-mercaptopyruvate sulfurtransferase and produces hydrogen sulfide. J Biochem 2009; 146:623-6.
56. Olson KR. *The therapeutic potential of hydrogen sulfide: Separating hype from hope.* Vol 3012011.
57. Yang GD, Wu LY, Jiang B, Yang W, Qi JS, Cao K, et al. H(2)s as a physiologic vasorelaxant: Hypertension in mice with deletion of cystathionine gamma-lyase. Science 2008; 322:587-90.
58. Cheng YQ, Ndisang JF, Tang GH, Cao K, Wang R. Hydrogen sulfide-induced relaxation of resistance mesenteric artery beds of rats. Am J Physiol-Heart Circul Physiol 2004; 287:H2316-H23.
59. Madden JA, Ahlf SB, Dantuma MW, Olson KR, Roerig DL. *Precursors and inhibitors of hydrogen sulfide synthesis affect acute hypoxic pulmonary vasoconstriction in the intact lung.* Vol 1122012.

60. Kubo S, Doe I, Kurokawa Y, Nishikawa H, Kawabata A. Direct inhibition of endothelial nitric oxide synthase by hydrogen sulfide: Contribution to dual modulation of vascular tension. Toxicology 2007; 232:138-46.
61. Cheang WS, Wong WT, Shen B, Lau CW, Tian XY, Tsang SY, et al. 4-aminopyridine-sensitive k+ channels contributes to nahs-induced membrane hyperpolarization and relaxation in the rat coronary artery. Vasc Pharmacol 2010; 53:94-98.
62. Chai Q, Lu T, Wang XL, Lee HC. Hydrogen sulfide impairs shear stress-induced vasodilation in mouse coronary arteries. Pflugers Arch 2014; 6:6.
63. Hedegaard ER, Nielsen BD, Kun A, Hughes AD, Kroigaard C, Mogensen S, et al. K(v)7 channels are involved in hypoxia-induced vasodilatation of porcine coronary arteries. Br J Pharmacol 2014; 171:69-82.
64. Casalini ED, Goodwill AG, Owen MK, Moberly SP, Berwick ZC, Tune JD. Contribution of hydrogen sulfide to the control of coronary blood flow. Microcirculation 2013; 20:12083.
65. Li L, Bhatia M, Zhu YZ, Zhu YC, Ramnath RD, Wang ZJ, et al. Hydrogen sulfide is a novel mediator of lipopolysaccharide-induced inflammation in the mouse. The FASEB Journal 2005.
66. Wang YF, Zhao X, Jin HF, Wei HL, Li W, Bu DF, et al. Role of hydrogen sulfide in the development of atherosclerotic lesions in apolipoprotein e knockout mice. Arterioscler Thromb Vasc Biol 2009; 29:173-U71.
67. Wikstrom J, Gronros J, Gan LM. Adenosine induces dilation of epicardial coronary arteries in mice - relationship between coronary flow velocity reserve and coronary flow reserve in vivo using transthoracic echocardiography. Ultrasound Med Biol 2008; 34:1053-62.
68. Nagahara N, Nishino T. Role of amino acid residues in the active site of rat liver mercaptopyruvate sulfurtransferase - cdna cloning, overexpression, and site-directed mutagenesis. J Biol Chem 1996; 271:27395-401.
69. Ishii I, Akahoshi N, Yu XN, Kobayashi Y, Namekata K, Komaki G, et al. Murine cystathionine gamma-lyase: Complete cdna and genomic sequences, promoter activity, tissue distribution and developmental expression. Biochem J 2004; 381:113-23.
70. Kondo K, Bhushan S, King AL, Prabhu SD, Hamid T, Koenig S, et al. H2s protects against pressure overload–induced heart failure via upregulation of endothelial nitric oxide synthase. Circulation 2013; 127:1116-27.
71. Huang S, Chua JH, Yew WS, Sivaraman J, Moore PK, Tan CH, et al. Site-directed mutagenesis on human cystathionine-gamma-lyase reveals insights into the modulation of h2s production. J Mol Biol 2010; 396:708-18.
72. Zhu WD, Lin A, Banerjee R. Kinetic properties of polymorphic variants and pathogenic mutants in human cystathionine gamma-lyase. Biochemistry 2008; 47:6226-32.
73. Aird WC. Phenotypic heterogeneity of the endothelium: Ii. Representative vascular beds. CircRes 2007; 100:174-90.
74. Ali MY, Ping CY, Mok YYP, Ling L, Whiteman M, Bhatia M, et al. Regulation of vascular nitric oxide in vitro and in vivo; a new role for endogenous hydrogen sulphide? Br J Pharmacol 2006; 149:625-34.
75. King AL, Polhemus DJ, Bhushan S, Otsuka H, Kondo K, Nicholson CK, et al. Hydrogen sulfide cytoprotective signaling is endothelial nitric oxide synthase-nitric oxide dependent. Proceedings of the National Academy of Sciences 2014; 111:3182-87.
76. Whiteman M, Li L, Kostetski I, Chu SH, Siau JL, Bhatia M, et al. Evidence for the formation of a novel nitrosothiol from the gaseous mediators nitric oxide and hydrogen sulphide. Biochem Biophys Res Commun 2006; 343:303-10.
77. Hayes JD, McMahon M. Nrf2 and keap1 mutations: Permanent activation of an adaptive response in cancer. Trends Biochem Sci 2009; 34:176-88.

78. Ma ZC, Hong Q, Wang YG, Tan HL, Xiao CR, Liang QD, et al. Ferulic acid protects human umbilical vein endothelial cells from radiation induced oxidative stress by phosphatidylinositol 3-kinase and extracellular signal-regulated kinase pathways. Biol Pharm Bull 2010; 33:29-34.
79. Khan NM, Sandur SK, Checker R, Sharma D, Poduval TB, Sainis KB. Pro-oxidants ameliorate radiation-induced apoptosis through activation of the calcium-erk1/2-nrf2 pathway. Free Radic Biol Med 2011; 51:115-28.
80. Benavides GA, Squadrito GL, Mills RW, Patel HD, Isbell TS, Patel RP, et al. Hydrogen sulfide mediates the vasoactivity of garlic. Proceedings of the National Academy of Sciences 2007; 104:17977-82.
81. Bucci M, Vellecco V, Cantalupo A, Brancaleone V, Zhou Z, Evangelista S, et al. Hydrogen sulfide accounts for the peripheral vascular effects of zofenopril independently of ace inhibition. Cardiovasc Res 2014; 102:138-47.

MAGGIE M. KUO

EDUCATION

Johns Hopkins University *December 2014*
Ph.D., Biomedical Engineering

University of California, San Diego *June 2008*
B.S., Bioengineering
GPA: 3.855 of 4.0, *magna cum laude*

RESEARCH EXPERIENCE

Graduate Researcher, **Johns Hopkins University**, Baltimore, MD *2/2009 – 8/2014*
Advisor: Dan E. Berkowitz
Thesis title: Vasoactive mediators underlying coronary tone regulation and dysregulation

- Developed novel techniques using ultrasound imaging to measure coronary vasodilatory function and aortic stiffness *in vivo* in rat and mouse models
- Characterized effects of ionizing radiation exposure on coronary artery function to investigate pathogenesis of and potential targets of intervention to radiation-associated coronary artery disease
- Investigated role of hydrogen sulfide and its vascular sources, cystathionine gamma lyase and 3-mercaptopyruvate sulfurtransferase, in modulating coronary artery tone
- Trained and mentored undergraduates and research fellows in vascular biology experimental procedures

Undergraduate Research Assistant, **University of California, San Diego**, La Jolla, CA *2/2007 – 3/2008*
Advisor: Geert W. Schmid-Schonbein

- Investigated effects of fluid shear stress on macrophage adhesion function
- Isolated and cultured macrophages from volunteer blood samples, performed *in vitro* shear experiments and data analysis

Undergraduate Research Assistant, **University of California, San Diego**, La Jolla, CA *1/2006 – 12/2006*
Advisor: Andrew D. McCulloch

- Contributed to project investigating genetic basis of cardiac response to hypoxia
- Carried out *Drosophila* breeding and heart rate data collection

PUBLICATIONS

Kuo MM, Pandey DR, Bergman Y, Abraham TP, Shoukas AA, Santhanam L, Berkowitz DE. MPST and not CSE is the primary regulator of hydrogen sulfide production and function in the coronary artery. *Am J Physiol-Heart C*. (In revision)

Kuo MM, Park JT, Kim JH, Santhanam L, Abraham TP, Shoukas AA, Berkowitz DE. Early effects of ionizing radiation on coronary artery function *in vivo*. *J Vasc Res*. (In review)

Kuo MM, Barodka V, Abraham TP, Steppan J, Shoukas AA, Butlin M, Avolio A, Berkowitz DE, Santhanam L. (2014) Measuring ascending aortic stiffness *in vivo* using high-resolution ultrasound. *J Vis Exp*. 94: e52200.

Soucy KG, Lim HK, Kim JH, Oh Y, Attarzadeh DO, Sevinc B, **Kuo MM**, Shoukas AA, Vazquez ME, Berkowitz DE. (2011) HZE (56)Fe-ion irradiation induces endothelial dysfunction in rat aorta: role of xanthine oxidase. *Radiat Res*. 176: 474-85.

Santhanam L, Tuday EC, Webb AK, Dowzicky P, Kim JH, Oh YJ, Sikka G, **Kuo M**, Halushka MK, Macgregor AM, Dunn J, Gutbrod S, Yin D, Shoukas A, Nyhan D, Flavahan NA, Belkin AM, Berkowitz DE. (2010) Decreased

S-nitrosylation of tissue transglutaminase contributes to age-related increases in vascular stiffness. *Circ Res*. 107: 117-25.

CONFERENCE PRESENTATIONS

Kuo MM, Santhanam L, Abraham TP, Shoukas AA, Berkowitz DE. Ionizing Radiation Exposure Alters Coronary Vascular Function. 2013 IAA Humans in Space Symposium. Cologne, Germany. (*oral)*

Kuo MM, Abraham TP, Shoukas AA, Berkowitz DE. ROS Mediates Radiation-Induced Coronary Vascular Dysfunction. 2013 NASA Human Research Program Investigators' Workshop, Galveston, TX. (*oral)*

Kuo MM, Santhanam L, Abraham TP, Shoukas AA, Berkowitz DE. Ionizing Radiation Exposure Alters Coronary and Cardiac Function. 2013 Experimental Biology, Boston, MA. *(poster)*

Kuo MM, Shoukas AA, Berkowitz DE. Endothelial Repair after Low-dose Ionizing Radiation Injury. 2012 NASA Human Research Program Investigators' Workshop, Houston, TX. *(poster)*

Kuo MM, Mac Gabhann F, Shoukas AA, Berkowitz DE. Low-dose Ionizing Radiation and Cardiovascular Health. 2011 IAA Humans in Space, Houston, TX. *(poster)*

Kuo MM, Soucy KG, Shoukas AA, Berkowitz DE. Time and dose effects of low-dose iron radiation on vascular function. 2010 NASA Space Radiation Investigators' Workshop, Port Jefferson, NY. *(poster)*

Kuo MM, Soucy KG, Shoukas AA, Berkowitz DE. Low-dose iron radiation impairs vessel function. 2010 NASA Human Research Program Investigators' Workshop, Houston, TX. *(poster)*

TEACHING

Instructor, Physiology for Applied Biomedical Engineering, Johns Hopkins University	*11/2013*
Instructor, Systems Bioengineering Lab I, Johns Hopkins University	*10/2013*
Instructor, Physiology Lab for Applied BME, Johns Hopkins University	*9/2012 – 12/2012*
Teaching Assistant, Systems Bioengineering Lab I, Johns Hopkins University	*9/2011 – 10/2011*
Teaching Assistant, Systems Bioengineering I, Johns Hopkins University	*10/2010 – 12/2010*

ADDITIONAL EXPERIENCE

Intern Science Writer, **ASBMB**, Rockville, MD *9/2014 – 01/2015*

- Wrote for the monthly magazine of the American Society for Biochemistry and Molecular Biology, *ASBMB Today*
- Wrote science news articles on recent publications in the society's journals *Molecular & Cellular Proteomics* and *Journal of Biochemistry*
- Wrote profiles on society members and articles on science outreach efforts

Intern Analyst, **Acidophil LLC**, Baltimore, MD *6/2013 – 3/2014*

- Interned with venture firm that founds and develops biotechnology companies
- Surveyed scientific publications and patents to determine the current state of knowledge and technology for biological-based production of 3 industrial chemicals
- Prepared small business grant applications and presentations for meetings with industrial collaborators

Volunteer Tutor, **Greater Homewood Adult Learning Center**, Baltimore, MD *8/2012 – 8/2013*

- Prepared one student in essay writing for GED high school equivalency exam. Taught student how to effectively structure and organize an essay. This student successfully passed the GED exam.
- Taught phonics to another student to improve basic reading skills